Republic of Iraq

Ministry of Higher Education and

Scientific Research

University of Babylon

College of Materials Engineering

Department of Ceramic Engineering

and Building Materials

Investigation of structural and electrical properties of PZT ceramics modified with donor and acceptor dopants

A Thesis
Submitted to College of Materials Engineering/ University of Babylon in Partial Fulfillment of the Requirements for the High Diploma Degree in Materials Engineering/ Ceramic Engineering

by
Abdulmajeed Hameed Uqla
(B.Sc. In Ceramic Engineering and Building Materials, 2019)

Supervised by
Dr. Mohammed Naji Al-Aaraji

2022 A.D **1443 A.H**

بِسْمِ اللَّهِ الرَّحْمَٰنِ الرَّحِيمِ

يَرْفَعِ اللَّهُ الَّذِينَ آمَنُوا مِنكُمْ وَالَّذِينَ أُوتُوا الْعِلْمَ دَرَجَاتٍ

سورة المجادلة – الآية 11

صدق الله العلي العظيم

Certification

I certify that, this thesis entitled **"*Investigation of structure and microstructure properties of PZT ceramics modified with donor and acceptor dopants*",** is prepared by "***Abdulmajeed Hameed Uqla***" under my supervision at the University of Babylon/ College of Materials Engineering/ Department of Ceramic Engineering and Building Materials in partial fulfillment of the requirements for the degree of Higher Diploma in Materials Engineering/ Ceramic Engineering.

(Supervisor)

Signature:

Name: Mohammed Naji Hassan Al-Aaraji

Date: / / 2022

Examination Committee Certification

We certify that we had read this thesis entitled **(Investigation of structural and electrical properties of PZT ceramics modified with donor and acceptor dopants)** and as an Examination Committee, we examined the student (**Abdulmajeed Hameed Uqla)** in its contents and that in our opinion it meets the standard of a thesis and is adequate for the award of the Degree of High Diploma in Materials Engineering/ Ceramic.

Signature:
Asst. Prof. Firas Jabbar Hmood
University of Babylon
Date: / /2022
(Chairman)

Signature:
Lecture Kutaiba AL-Marzoki
University of Babylon
Date: / /2022
(Member)

Signature:
Dr. Mohammed Naji Al-Aaraji
University of Babylon
Date: / /2022
(Supervisor)

Head of Ceramics and Building Materials Engineering Department

Signature:
Prof. Dr. Mohsin Abbas Aswad
Date:

Dean of College of Materials Engineering

Signature:
Prof. Dr. Imad A. Disher
Date:

Dedication

To:

The one who paved the way for me, dear brother Ghassan

To the person who supported me all the way, my wife.

Acknowledgments

First and foremost, I would like to convey my heartfelt thanks and gratitude to my supervisor, Dr. Mohammed Naji Al-Aaraji, for his invaluable advice and unwavering support during my high diploma research. He not only shared his expertise and vast experience, but he also provided me with unending support and confidence whenever I needed it.

I would also like to extend my sincere thanks to the head of the department, Dr. Mohsen, and all the professors working in the laboratories for their cooperation in conducting the examinations and providing the supplies

also, I want to thank all my friends and family who contributed to providing great moral support, especially dear friend and brother Ghassan Bashir, respected Dr. Faisal director of Alkafeel Omnnea company, and my project manager Mr. Naael for giving me the opportunity to complete the projec

Content

Contents

Table of Figures

Abbreviations and Symbols

Abbreviation	Name	Formula
AC	Alternating current	
MPB	Morphotropic Phase Boundary	
NF	Normal ferroelectric	
P-E	Polarisation-electric field	
PEG	Polyethylene glycol	
PLZT	Lead Lanthanum Zirconate Titanate	$(Pb,La)(Zr\ Ti,)O_3$
PZT	Lead zirconate titanate	$(Pb)(Zr,Ti,)O_3$
RF	Relaxor ferroelectric	
SEM	Scanning Electron Microscopy	
XRD	X-Ray diffraction	
Symbols	Name	
(h k l)	Miller indices	
a, b, c	Lattice parameter	
a.u.	arbitrary unit	
C	capacitance	
E	electric field	
E_c	coercive electric field	
I	Current	
P	polarisation	
P_r	remnant polarisation	
P_s	spontaneous polarisation	
Q	electrical charge	

R_A	Ionic radius for A-site atom in perovskite	
R_B	Ionic radius for B-site atom in perovskite	
R_O	Ionic radius for O-site atom in perovskite	
t	Perovskite tolerance factor	
tanδ	Dielectric loss tangent	
T_C	Curie temperature	
V	voltage	
Θ	Bragg's angle	
λ	X-ray wavelength	
ρ	Density	
ε_r	Relative dielectric permittivity	
d_{33}	polarization in direction z axis per unit stress applied in z axis.	

Abstract

Lead-based (PZT) ferroelectric ceramic materials were prepared utilizing solid state reaction method as a pure and doped with different additives. As a pure form, the composition with chemical formula $Pb_{1.03}(Zr_{0.56}Ti_{0.44})O_3$ that characterized with rhombohedral structure according to PZT phase diagram region, was investigated systematically. Afterwards, different strategies of doping were followed to investigate the influence of donor and acceptor ion in addition to complex doping on structural and microstructure properties of the parent composition. For the soft ceramic, 2 mol% lanthanum-doped PZT at A-site, whereas 2 mol% of Scandium-doped PZT at B-site to produce hard ceramic. In terms of complex doping, 2 mol% of both La^{+3} and Sc^{+3} substitute A- and B- site, respectively.

All samples show dense and homogeneous microstructures ceramics exempt PSZT ceramic displays small grain size, relatively. XRD results show that the addition of Sc^{+3} induce phase transformation and formation coexistence region consist of tetragonal and rhombohedral phases. This region was recognized in both compositions (PSZT) (PLSZT). Hard ceramic (Sc^{+3} doped PZT) exhibited highest values (around 3450) of relative permittivity and lowest dielectric loss (around 0.007) at frequency of 100 kHz.

Chapter One

Introduction and objective

1 Introduction and objectives

1.1 Introduction

Ferroelectric materials have spontaneous electric polarization that may be reoriented between crystallographically defined states by applying an external electric field. Due to the pyroelectric nature of the materials, the amplitude or direction of spontaneous polarization may be adjusted as a function of pressure, temperature, frequency, or applied fields[1] Because of these materials' unique properties, they are suited for a broad range of applications[2], many of which are connected to electronics or biological applications. Ferroelectric materials are frequently employed in memory applications [3].Ferroelectric relaxer materials. And antiferroelectric materials, on the other hand, are more commonly utilized in energy-storage applications. The need for high-power energy storage has increased dramatically in recent years due to the fast advancement of electronic gadgets and power systems. Dielectric capacitors with high energy-storage densities have received a lot of interest due to their numerous electronic uses in wind turbines, lasers, medical defibrillators, and so on[4]. Dielectric ceramic capacitors feature high power density, nanoscale charge/discharge time, and $>10^6$ cycle cycling dependability. The relaxor ferroelectrics, with their slim polarization electric field hysteresis (P-E) loop, produce large charge/discharge energies. Relaxor behavior in ferroelectrics may be accomplished by frustration or compositionally induced disorder, and it is one of the most active current study topics for energy-storage applications[5].

This paper focuses on the structural and electrical properties of ceramic compounds $Pb_{1.03}(Zr_{0.56}Ti_{0.44})O_3$ .The composition was doped with 2% Lanthanum (La^{3+}) as a donor dopant at the A-site ($Pb_{0.98}$ $La_{0.02}$) ($Zr_{0.56}Ti_{0.44}$) O_3 [PLZT] and 2% Scandium (Sc^{3+}) as an acceptor dopant at the B-site Pb

($Sc_{0.02}$ $Zr_{0.54}$ $Ti_{0.44}$) O_3 [PSZT]. Furthermore, co-doping with 2% Lanthanum and Scandium ($Pb_{0.98}$ $La_{0.02}$) ($Sc_{0.02}$ $Zr_{0.54}$ $Ti_{0.44}$) O_3 [PL-SZT]. We study the effect of La^{3+} and Sc^{3+} substitution on PZT as a donor, acceptor, and co-doping on structural and electrical properties of PZT ceramic.

1.2 Study objectives

The main goal of this project was to obtain optimized PZT ferroelectric around MPB region in term of structural and electrical properties throughout doping. For this purpose, we propose that the doping in PZT composition close to MPB region, could help to cause a phase transformation which can be employed in different applications. Therefore, the dopants ions will substitute the Zr^{+4} and Pb^{+2} sites.

To achieve this objective, the project was divided into three stages: the first was to make the doping at A-site using La^{+3} ion to substitute Pb^{+2} as a donor.

The aim of the second stage was the doping at B-site using Sc^{+3} ion to substitute Zr^{+4} as acceptor. That can help to induce phase transformation due to decreasing the Zr^{+4} ions that stabilize the rhombohedral region.

The final stage is concerned with complex doping by conduction the first two stages.

Finally, the prepared undoped and doped samples are characterized using XRD and SEM techniques to investigate the influence of parent composition and doping ions on the structure and microstructure properties. Furthermore, functional characterization of the produced ceramics should be achieved, including relative permittivity, dielectric breakdown, conductivity and P-E hysteresis loops to evaluate the possibility of using them in electrical applications.

Chapter Two

Background and literature review

2 Background and literature review

This chapter contains the basic concepts related to ferroelectric ceramics, from the group of ferroelectrics, PZT was chosen to study the effect of doping using (La^{3+}, Sc^{3+}, and co-doping La^{3+}-Sc^{3+}) on the physical and electrical properties. The methods of powder and samples production were explained, with a focus on the solid-state reaction route, as well as the most important applications were presented.

2.1 The perovskite structure

The word perovskite comes from the mineral $CaTiO_3$ perovskite. Perovskite is a ternary chemical having the formula ABO_3 with different-sized A and B cations. A face-centered cubic (FCC) lattice is formed by the bigger A cation and oxygen, while the smaller B cation occupies the octahedral interstitial spaces in the array. The structure is made up of a network of corner-linked oxygen octahedra. The dodecahedral holes are filled with massive cations, whereas the octahedral holes are filled with little ones. A cubic perovskite structure is shown in Figure 2-1 [6]. The perovskite-type structure may be found in a variety of valuable ferroelectric oxide materials, including (Lead titanate ($PbTiO_3$)), (Barium titanate ($BaTiO_3$)), (Potassium niobate ($KNbO_3$)), and (lead zirconate titanate ($Pb(Zr,Ti)O_3$))[7].On the A and B sites, the perovskite structure accommodates a wide spectrum of ions. A-site cations have valences ranging from +1 to +3 (for example, Ba^{2+}), whereas B-site cations have valences ranging from +2 to +6 (for example, Ti^{4+}). The tolerance factor (t) was developed by Goldschmidt as a measure of deformation of the prototype perovskite structure that demonstrates the stability of a compound. The tolerance factor is computed as follows:

$$t = \frac{R_A + R_O}{\sqrt{2}(R_B + R_O)} \quad (2\text{-}1)$$

Where:

R_A: ionic radii of the A-site atom.

R_B: ionic radii of the B-site atom.

R_O: ionic radii of the oxygen atoms.

The structure of the perovskite can be identified by tolerance values in the range ($0.88 \leq t \leq 1.09$)[8].

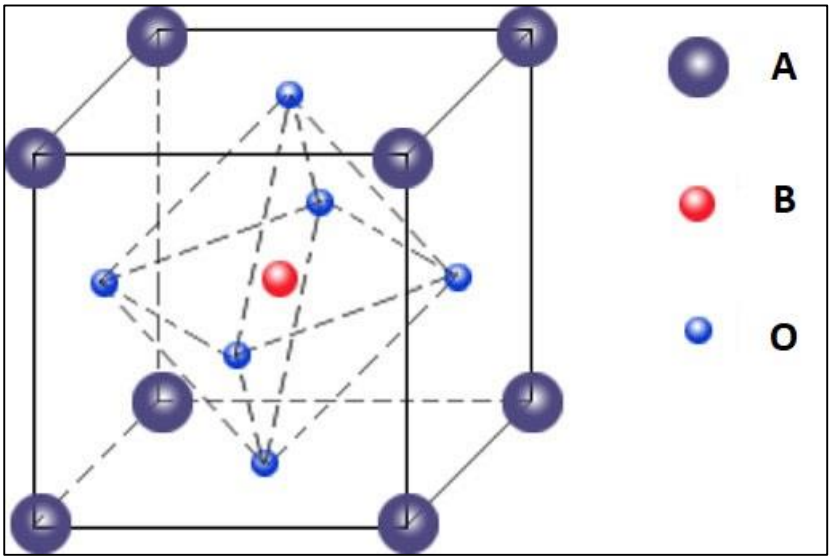

Figure 2-1 Schematic diagram of the ABO_3 perovskite structure[8].

2.2 Electroceramics

Electroceramics are advanced ceramic materials utilized in electrical, optical, and magnetic applications. They have previously had a significant influence on the electronic revolution. They are now used in micro-electromechanical system devices as a result of advances in thin-film deposition methods to produce materials at the micro-scale with regulated stoichiometry and the integration of electroceramic functionalities with microelectronics[9].

Microstructure is the response to electroceramic properties. and all crystals may be divided into 32 unique classes. These are point groups that are divided by the symmetry components listed below: (i) center of symmetry, (ii) mirror planes, (iii) rotation axes, and (iv) different combinations of these. [10]. The 32-point groups are subsets of seven basic crystal systems: cubic, hexagonal, monoclinic, triclinic, tetragonal, rhombohedral (trigonal), and orthorhombic. Piezoelectricity exists in twenty of the 21 noncentrosymmetric classes of the 32-point groups, which is a required requirement for the presence of piezoelectricity. Pyroelectric properties are present in ten of the twenty piezoelectric crystal classes. Figure 2-2. This category of materials is permanently polarized within a particular temperature range. Unlike typical piezoelectric polarization, pyroelectric polarization forms spontaneously and is preserved as permanent dipoles in the structure. The reaction is known as pyroelectricity because the polarization changes with temperature.[10].

The perovskite family of materials is useful in various electroceramic applications, including ferroelectric, pyroelectric, piezoelectric, superconductive, thermoelectric, dielectric, magnetic, linear, and nonlinear electro-optic devices. Because lead zirconate titanate perovskites are ferroelectric, they can be poled in an electric field. Poling aligns the dipoles to provide a high piezoelectric response, which means that the applied pressure is converted into an electric signal[9].

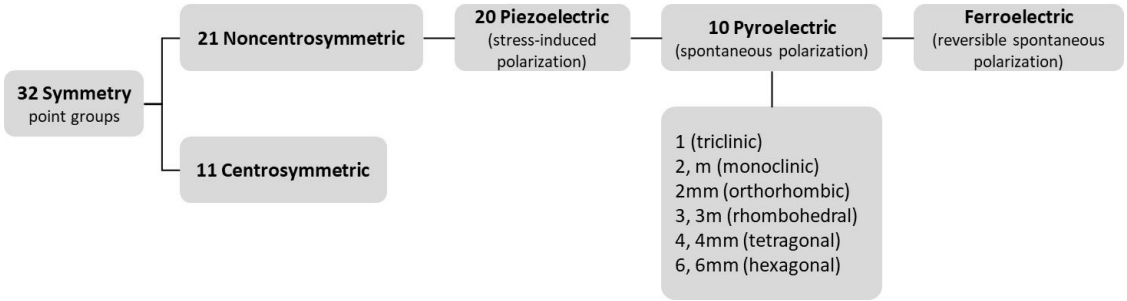

Figure 2-2 Hierarchy of symmetry relations in dielectric crystals.

2.2.1 Dielectric ceramics

Dielectrics are characterized by high electrical resistivity, which enables them to be used as electrical insulators. An ideal dielectric does not conduct electric charge when exposed to an electric field, E. Instead, it becomes polarized because of the separation of opposite charges over a certain distance, creating a dipole moment. In other words, the dielectric possesses a polarization, *P*, which is defined as the net dipole moment (*p*) per unit volume (*V*). *P* is measured in units of C m/m^3 = C m^{-2}. There are four primary polarization mechanisms: atomic or electronic, ionic, dipolar, and space charge or diffusional. [11], as illustrated in Figure 2-3.Each mechanism has its own characteristic response time, which leads to the schematic frequency-dependence of dielectric permittivity illustrated in Figure 2-4

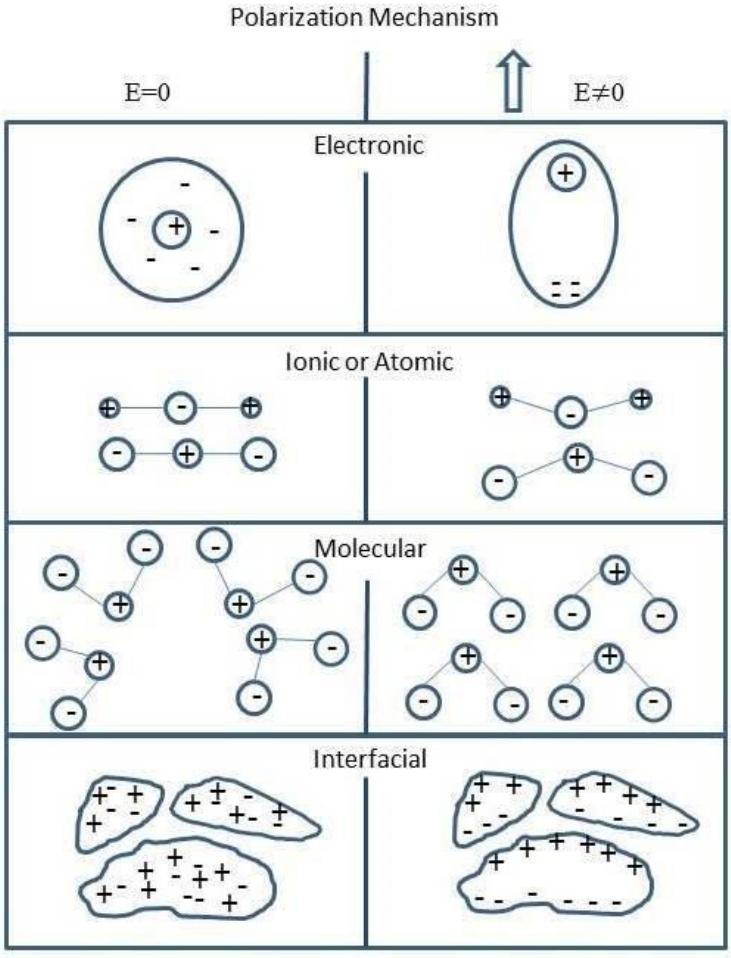

Figure 2-3 Schematic representation of different mechanism of polarization[12]

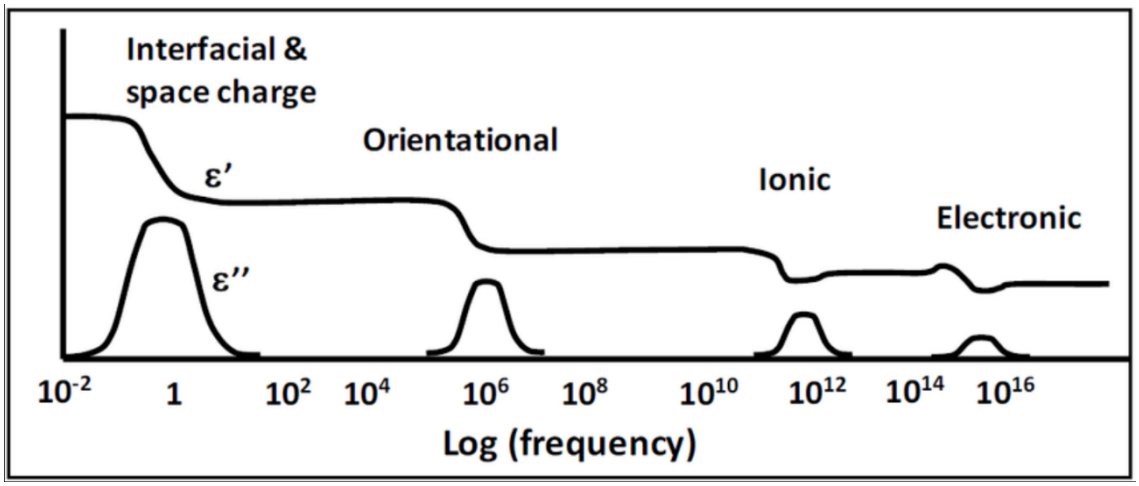

Figure 2-4. Schematic illustration of variations in dielectric constant ε_r' and loss ε_r'' as a function of frequency[12]

2.3 Dielectric properties

2.3.1 Relative permittivity and capacitance

The dielectric constant or relative permittivity, dielectric loss, and dielectric strength are the most important parameters for dielectrics. However, it is first required to define how polarization is measured and the link between polarization and dielectric characteristics.

Consider two metallic parallel plates (i.e., a capacitor) separated in vacuum by a distance, d, as illustrated in Figure 2-5(a). When an electric field is applied, the charges (Q) are spread equally over the plates' opposing surfaces.

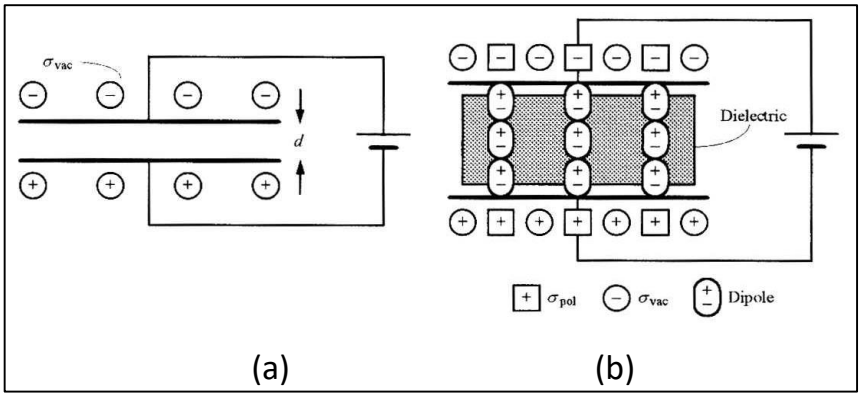

Figure 2-5. Diagrams of a parallel-plate capacitor that demonstrate how charge may be held on the capacitor plates in (a) vacuum and (b) with a dielectric material between the plates. [13]

According to equation 2-2, increasing the applied voltage, V, induces a linear increase in the stored charge, *Q*, as seen in Figure 2-6

$$\boldsymbol{Q = C.V} \qquad (2\text{-}2)$$

The slope of the *Q* versus *V* curve is the capacitance, C_o, (free space) of the parallel plates in vacuum, given by:

$$\boldsymbol{C_o = \frac{\varepsilon_o \cdot A}{d}} \qquad (2\text{-}3)$$

where ε_o is the permittivity of vacuum, ε_o = 8.85 x 10^{-12} F m^{-1} , and *A* is electrode area.

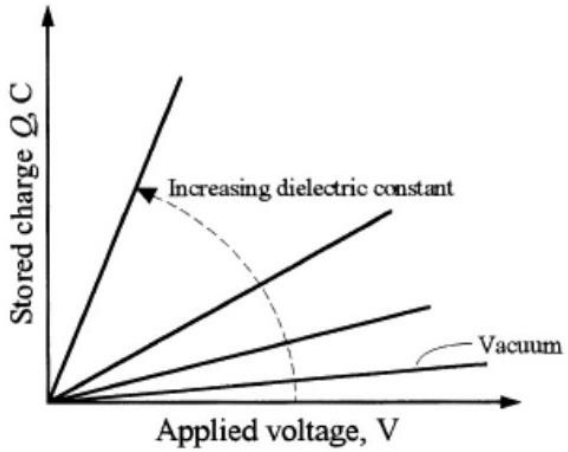

Figure 2-6. Functional dependence of Q on applied voltage. The gradient of each line equals the capacitance, which is proportional to the dielectric constant of the substance [13].

When a barrier is inserted between the plates, as shown in Figure 2-5(b), and an electric field is produced, the stored charge increases, as shown in Figure 2-6, where the slope of the *Q* - *V* curve is greater than in a vacuum. In other terms, Eq. (2.4) is changed as follows:

$$\boldsymbol{C = \frac{\varepsilon \cdot A}{d}} \qquad (2\text{-}4)$$

Where ε: *permittivity* of dielectric between the plates.

A material's relative permittivity, or dielectric constant, ε_r, is the ratio of a substance's permittivity to that of vacuum. As a result, it is a parameter with

no dimensions. Because ε is bigger than ε_o, The smallest possible value for ε_r is 1.

$$\boldsymbol{\varepsilon_r = \frac{\varepsilon}{\varepsilon_o}} \quad (2\text{-}5)$$

The dielectric permittivity of the material is also linked to a dimensionless constant known as the electric susceptibility, χ_e; this parameter governs the degree of polarization of a dielectric material in response to an applied electric field (see equation 2-8 below). As a result, the capacitance between the parallel plates increases by a factor of $(1+\chi_e)$, depending on the dielectric material used between them. According to Equations 2.6 and 2.7, the permittivity, and relative permittivity, are connected to the susceptibility.

$$\boldsymbol{\varepsilon = \varepsilon_o(1 + \chi_e)} \quad (2\text{-}6)$$

$$\boldsymbol{\varepsilon_r = (1 + \chi_e) = \frac{\varepsilon}{\varepsilon_o}} \quad (2\text{-}7)$$

Furthermore, the relationship between polarization and electric field is given by Equation 2-8 [11]

$$\boldsymbol{P = \chi_e \varepsilon_o E} \quad (2\text{-}8)$$

2.3.1.1 Dielectric loss

The dielectric loss of a substance in an alternating field is another significant feature of a dielectric. When an alternating voltage is supplied across an ideal dielectric, the phase of current, *I*, across the capacitor advances by an angle of 90°, as illustrated in Figure 2-7a.

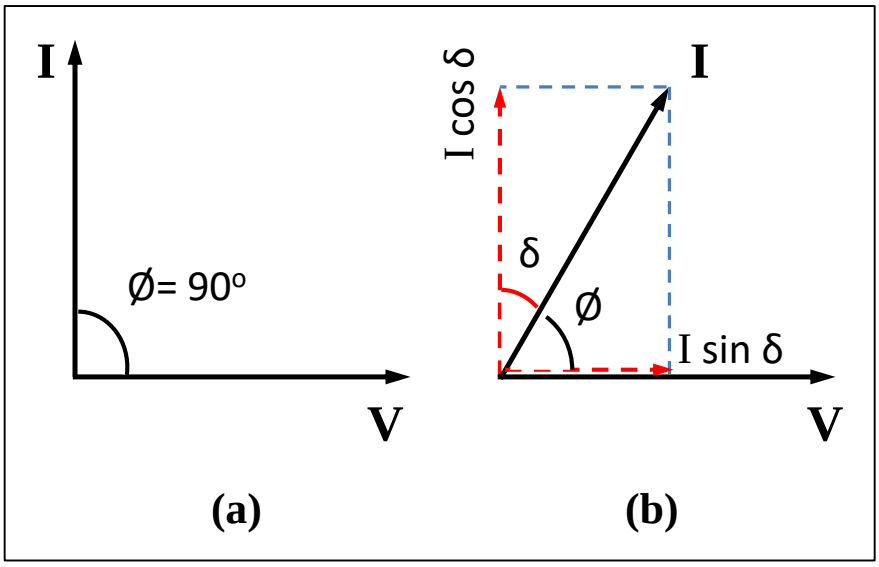

Figure 2-7. Representative diagram of (a) ideal dielectric and (b) real lossy dielectric , illustrating phase angle, ϕ, and loss angle, δ [13]

However, in the presence of a true lossy dielectric, the phase angle, ϕ, deviates from 90° because the polarization is no longer in phase with the applied voltage. In this instance, the resultant current is offset from the applied voltage by an angle ϕ= 90° - δ as illustrated in Figure 2-7 (b), where δ is known as the loss angle. The current may be divided into two parts: the *capacitive component*, which leads the applied voltage by 90°, and the *resistive component*, which is in phase with the applied voltage. The former is indicated by I cos δ and is the *imaginary* component of current, whereas the latter is designated by I sin δ and is the *real* component of current.

The quantity tan δ is used to calculate power loss. It is also known as the *dissipation factor* or *loss tangent*. According to equation 2-9, It is defined as the ratio of the dielectric constant's imaginary component, ε″, to the real component, ε′.

$$\boldsymbol{tan\,\delta} = \frac{\varepsilon''}{\varepsilon'} \qquad (2\text{-}9)$$

2.3.2 Dielectric Strength

The dielectric strength of an insulating substance is the voltage that it can withstand before breaking down. It is generally determined by the thickness of the material as well as the test technique and circumstances. Better insulating qualities are associated with higher dielectric strength.

Dielectric material breakdown occurs at an average potential per unit thickness. [14]. Whatever the case, The amount of electric field necessary to cause dielectric breakdown is defined as dielectric strength[15, 16]. When a strong electric field higher than the value of the specific critical is applied to an insulator, a relatively big electrical current is created, and the insulator's insulating characteristics are lost, and it becomes a conductor.[17]. The voltage that happens after the breakdown is referred to as (Breakdown Voltage). The dielectric strength equal to brackdown voltage divided by the sample thickness [18].As seen in the following equation [19]:

$$Dielectric\ strength = \frac{breakdown\ voltage}{insulator\ thickness}$$

$$E_{br} = \frac{U_{br}}{h}$$

$$U_{br} = E_{br}.\ h$$

Where:

E_{br}: Dielectric strength (KV/mm)

U_{br} : break down voltage.

h :insulator thickness.

Whenever highly intense electric fields are delivered through dielectric materials, a large number of electrons could be simultaneously accelerated to energies in the conduction band. Because of the movement of these

electrons, the current through the dielectric increases significantly; rarely, localized melting, burning, or vaporization causes irreversible damage and, in extreme cases, collapse of the material[20]. Material dielectric strength varies widely. Ceramic materials, for example, have an insulating strength of 1-20 kV/mm, while polymeric materials have an insulating strength of 20-50 kV/mm, which is hundreds of times that of conducting metals and alloys [15], Cracks, impurities, and pores can all lower dielectric strength. [18].

Viewing one of the following cases will reveal a breakdown in the material:

1. A hole in the sample happens when the insulator reaches its true electrical endurance.
2. When a substance is locally heated and breaks down, it is said to burn or melt. [21].

It should be noted that the dielectric strength of insulation varies based on where the applying voltage , (DC) provides (25-30%) higher values than the voltage (AC) at the frequency (60Hz), As in NaCl, the value of E_{br} ((3.8 * 10^4 kV/cm) in the (DC) whereas (1.4*10^3 kV/cm) in the (AC), and this discrepancy may be explained to relaxation loss. [22]. When an alternating voltage is given to an insulator, many events occur as a result of electrical conduction and polarization in the insulator, when the lead raises voltages on the insulator to improve the flow of capacitance current and leakage current for alternating voltage, it is at this moment that pass conduction current exists within the insulating material.

A circle is commonly used to indicate the source poles. The breakdown of a solid insulator defines all of the steps that the insulator goes through before breaking down and may be represented visually as three stages, as seen in Figure 2-8

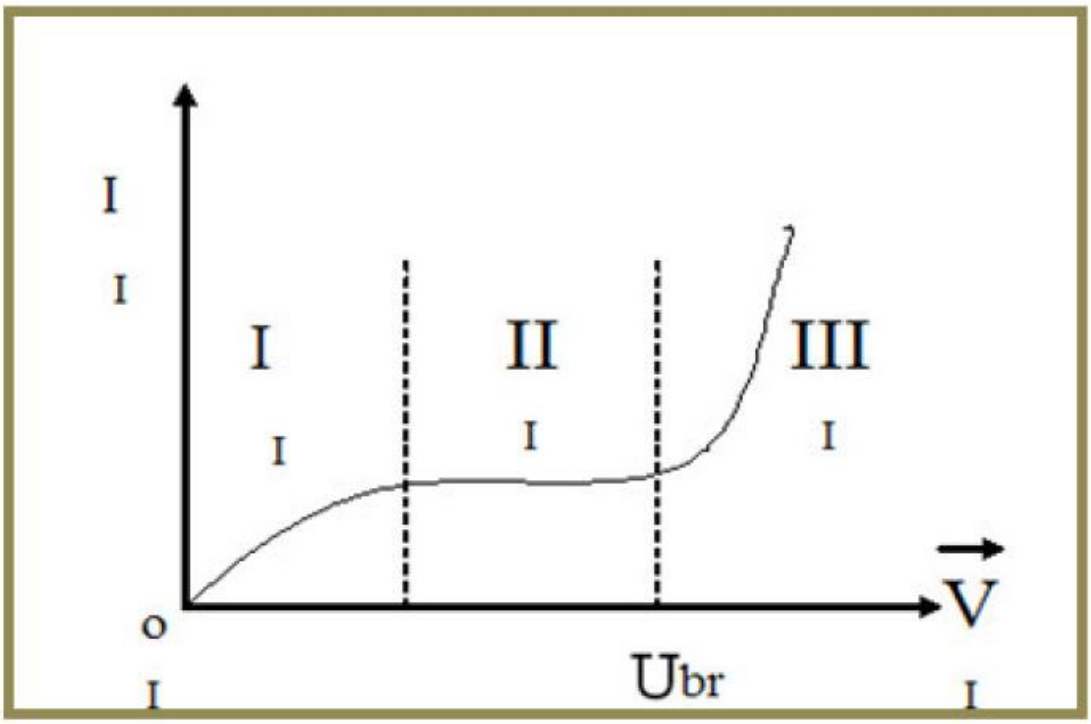

Figure 2-8 relationship between Current and Voltage In The Solid Insulators. [22]

The first: In the region (I), The relationship is linear according to Ohm's law, where the current increases linearly with increasing voltage until it reaches values no more than microamps.

The second: In the region (II), As the voltage increases, the current remains constant.

The third: In region (III), The current increases again at a certain voltage, which represents the beginning of the stage, which is the breakdown voltage (U_{br}) [22].

The failure method and breakdown strength vary with the time scale of voltage applied, therefore it is useful for discussion purposes to divide the time frame of voltage application into regions where separate mechanisms operate. [23]. As seen in Figure 2-9

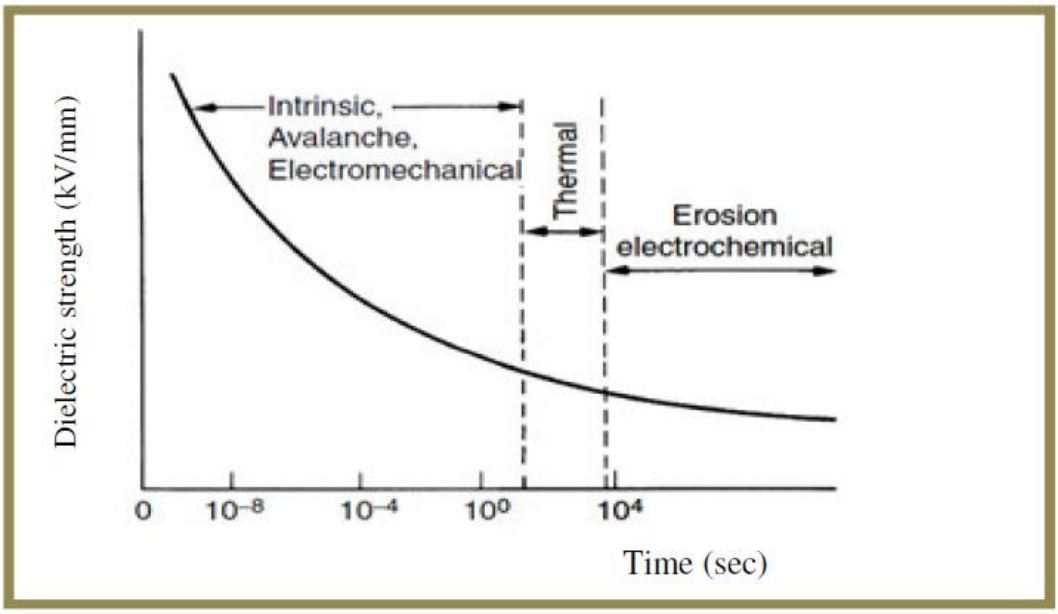

Figure 2-9 Failure Mechanisms and Variation of Breakdown Strength in Solids with Stressing Time [23]

2.3.3 The ferroelectric materials

The ferroelectric group is a subgroup of pyroelectric crystals that are spontaneously polarized. On the one hand, ferroelectric polarization is similar to that of pyroelectric. There is a contrast between the two polarizations, however, Because ferroelectric polarization may be reversed by an externally applied electric field, as long as the supplied field is smaller than the dielectric breakdown of the materials. As a result, ferroelectric materials must possess the following two characteristics:

1. the occurrence of spontaneous polarization
2. the polarization's reversibility in the presence of an electric field.

ferroelectric materials are pyroelectric, piezoelectric, and noncentrosymmetric.

2.3.3.1 Ferroelectricity and Antiferroelectricity

In terms of the depolarization process, ferroelectrics (FEs) and antiferroelectrics (AFEs) are closely related, thus they must be mentioned in order to comprehend the concept of antiferroelectrics (AFEs). Neighboring

diploes for one domain in FE materials share the same polarization orientation, and the diploes' orientation may be realigned with the aid of external DC electric field.[24]. As a result, FE materials must have two properties: (i) spontaneous polarization and (ii) polarization reversibility in the presence of an external electric field. Figure 2-10

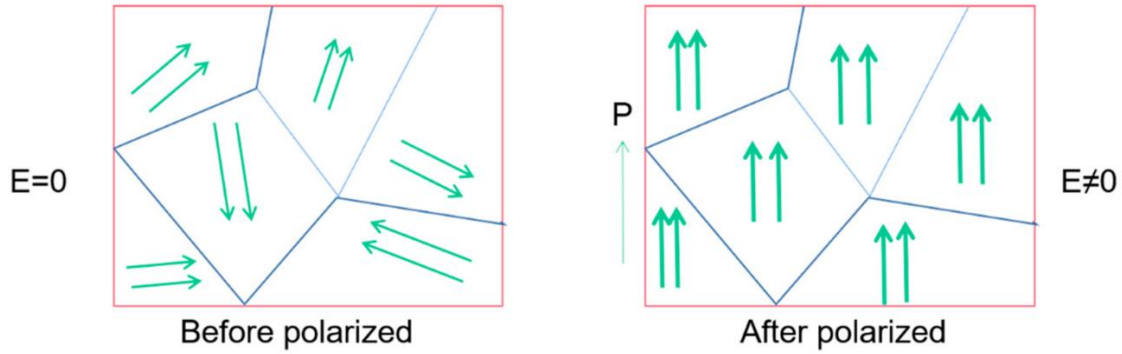

Figure 2-10 Schematic of the poling process in ferroelectric materials[25]

External DC electric fields can boost polarization in polycrystalline FE materials, causing them to behave similarly to single-crystalline FEs at saturated polarization. As a result, the electric-field dependence of polarization (P-E) of FEs is a single hysteresis loop, as shown in Figure 2-11. In AFE materials, neighboring diploes are oriented in the opposite direction. A sufficiently enough DC electric field is necessary in this scenario to align the polarization orientation of dipoles and establish a FE state. This phenomenon is referred to as electric-field-induced phase switching. AFEs, like FEs, have two distinct properties.

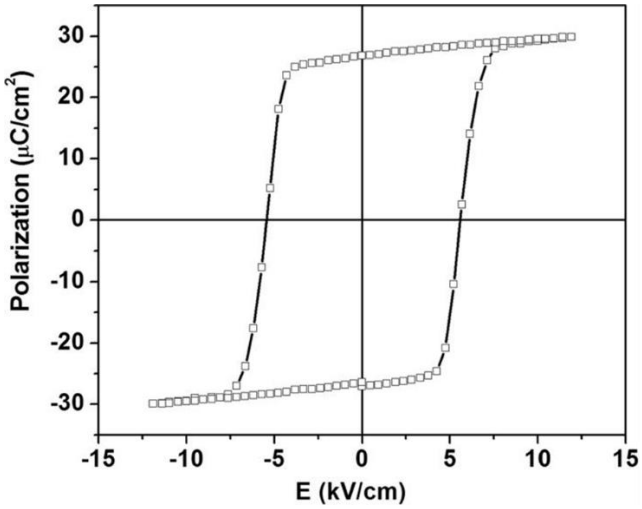

Figure 2-11 P-E hysteresis loop of FEs.[26]

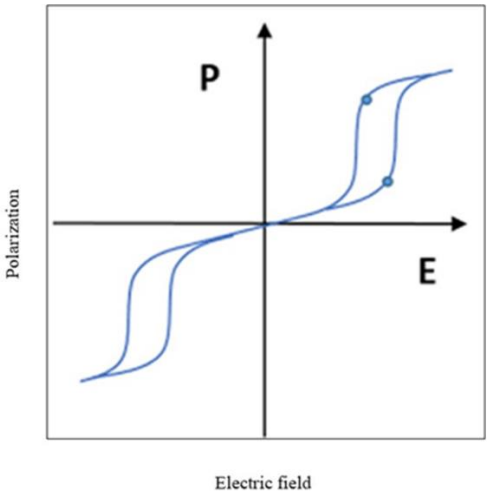

Figure 2-12 P-E hysteresis loop of AFEs [26]

On one hand, total remanent polarization is zero; on the other hand, P-E curves exhibit double hysteresis loops at sufficiently powerful electric fields.[27]. Figure 2-12 and Figure 2-13 show the polarization properties of the P-E loop and AFEs, respectively.

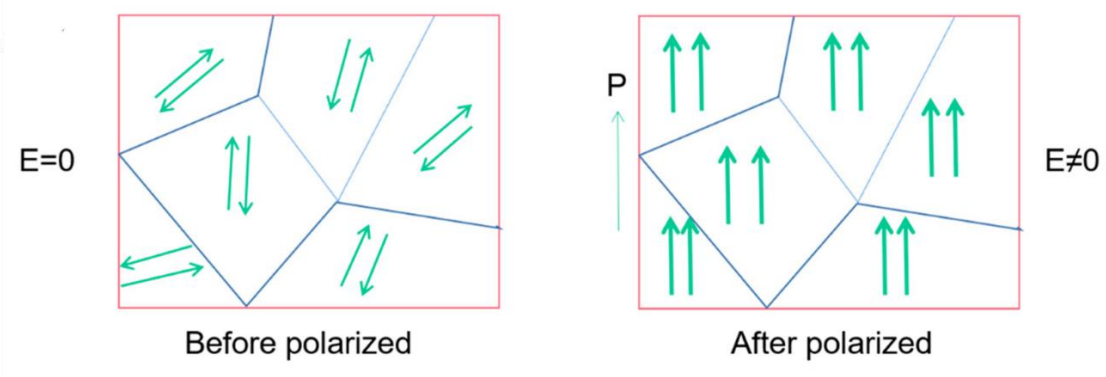

Figure 2-13 Diagram of polarization process of AFEs[25].

2.3.3.2 Lead- free ferroelectric materials

Due to the high lead concentration in PZT-based materials, In recent years, there has been a considerable effort to eliminate lead oxide as a component of piezoelectric ceramic devices. [28-31]. As a result, alternative lead-free piezoelectric ceramics must be developed in order to replace PZT in specific applications[32, 33]. The primary prospective ceramic materials for this purpose are $BaTiO_3$ (BT), $(K_{0.5}Na_{0.5})NbO_3$ (KNN), and $(Bi_{0.5}Na_{0.5})TiO_3$ (BNT) (BNT). Many studies on the manufacturing and characteristics of

these materials as pure compounds, modified by small dopants, or in solid solutions with other ABO3 perovskites have been done. [29, 34]. The current study will concentrate on PZT doped with soft and hard dopant.

2.3.3.3 Lead-based ferroelectric materials

Lead zirconate titanate (PZT) ceramic is the most widely used lead-based ferroelectric and piezoelectric material in industrial applications. Sawaguchi et al. discovered it about 1952 and it is still an important ferroelectric material [35, 36]. This is due to the fact that PZT compositions have high Curie point (T_C) that allows for high temperature operation (above 200 °C), high piezoelectric and electromechanical coupling coefficients, have a wide range of dielectric constants, can be easily poled, and form solid solutions with many different constituents, allowing for a wide range of achievable properties to meet the requirements of a specific application [37].

2.4 Lead Zirconate Titanate

Lead zirconate titanate, abbreviated Pb(Zr,Ti)O3 or PZT, has been the most economically successful ferroelectric system for more than fifty years. It has superseded BaTiO3 as the ferroelectric of choice for most technologies due to stronger electromechanical coefficients, a wider operating temperature range (i.e. greater Tc), and simpler poling and sintering processes. PZT properties may be easily changed to achieve remarkable dielectric, piezoelectric, pyroelectric, and electro-optic capabilities by generating a wide range of solid solutions containing various appropriate components. Its performance and tunability have benefitted nonvolatile memory (FeRAM), sensors, piezoelectric transducers, optoelectronic devices , and actuators[8].

PZT is a lead zirconate (PZ) and lead titanate (PT) solid solution. Figure 2-14 (a) depicts the phase diagram of a PZT solid solution. PZT has a cubic paraelectric phase structure at high temperatures. PZT exhibits a

ferroelectric or antiferroelectric phase below Tc. The morphotropic phase boundary (MPB) separates a tetragonal ferroelectric phase (the rich Ti part of the phase diagram) and a rhombohedral ferroelectric phase (the rich Zr region). At room temp. , the MPB's Ti:Zr ratio is 48:52 [7]. The dielectric and piezoelectric characteristics are greatly enhanced when the MPB is approached, as seen in Figure 2-14 (b)

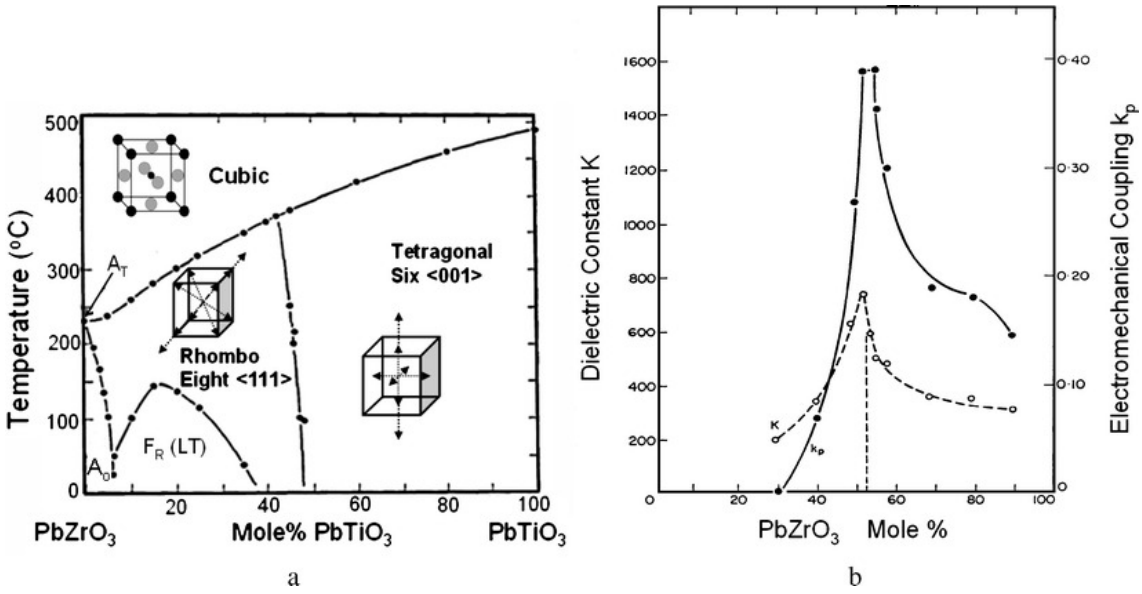

Figure 2-14 **(a)** Solid solution phase diagram of lead zirconate (PbZrO3) and lead titanate (PbTiO3). **(b)**: Peak of the relative dielectric constant (εr) and the planar electromechanical coupling coefficient (kp) at the MPB in PZT [38]

2.4.1 Doping in PZT system.

In order to tailor the composition of PZT, three types of additions were used. Table 2.1 summarizes the common additives and their impact on piezoelectric characteristics.

Table (2-1) Major effects of typical additives on the characteristics of PZT system

Additives	**Major Effects**
<u>Isovalent additives:</u> **Sr^{2+}(0.112) or Ba^{2+} (0.134) for Pb^{2+}(0.132)** **Sn^{4+} (0.071) for Ti^{4+} (0.079) or Zr^{4+} (0.068)**	Lower Curie point Higher permittivity
<u>Soft dopants:</u>	Higher permittivity Higher K_p

Nd^{3+} (0.115), La^{3+} (0.122), Bi^{3+} (0.114), Sb^{3+} (0.090) or Th^{4+} (0.110) for Pb^{2+} (0.132) **Nb^{5+} (0.069), Sb^{5+} (0.063), Ta^{5+} (0.068) or W^{6+} (0.065) for Ti^{4+} (0.068) or Zr^{4+} (0.079)**	Much Lower Q_m Resistivity about 10^3 higher
<u>Hard dopants:</u> **Na^{+} (0.094) or K^{+} (0.133) for Pb^{2+} (0.132)** **Al^{3+} (0.057), Fe^{3+} (0.067), In^{3+} (0.092), Sc^{3+} (0.083) or Cr^{3+} (0.064) for Zr^{4+} (0.079) or Ti^{4+} (0.068)**	Lower permittivity Lower dielectric loss Lower K_p Much higher Q_m

2.4.1.1 Soft doping

Soft PZT ceramics are made by doping donor ions like La^{3+} and Nd^{3+} (for site A) and Nb^{5+}, Sb^{5+} (for site B) into the lattice, resulting in vacancies on site A. High domain mobility and the resultant soft ferroelectric behavior are distinct advantages (easy to polarize). Moderate permittivity, the large piezoelectric charge coefficient, and high coupling factors of soft PZT materials make them attractive for actuators (micro and nano positioning), sensors such as ultrasonic transmitters, traditional vibration pickups, and receivers for flow or level measurement, and electro-acoustic applications such as microphones and sound transducers [39].

Concerning the soft doping, several papers have been studied. Caceres et al. investigated the effect of Erbium Er^{+3} on the electrical properties of PZT and discovered that Er^{+3} caused the sample's density to rise ($91.9\% < \rho < 99.0\%$) when compared to an undoped sample. In addition, The XRD spectra in Figure 2-15 are quite comparable, and our research indicates that the samples are monophasic, with peaks corresponding to tetragonal crystalline structure. [40].

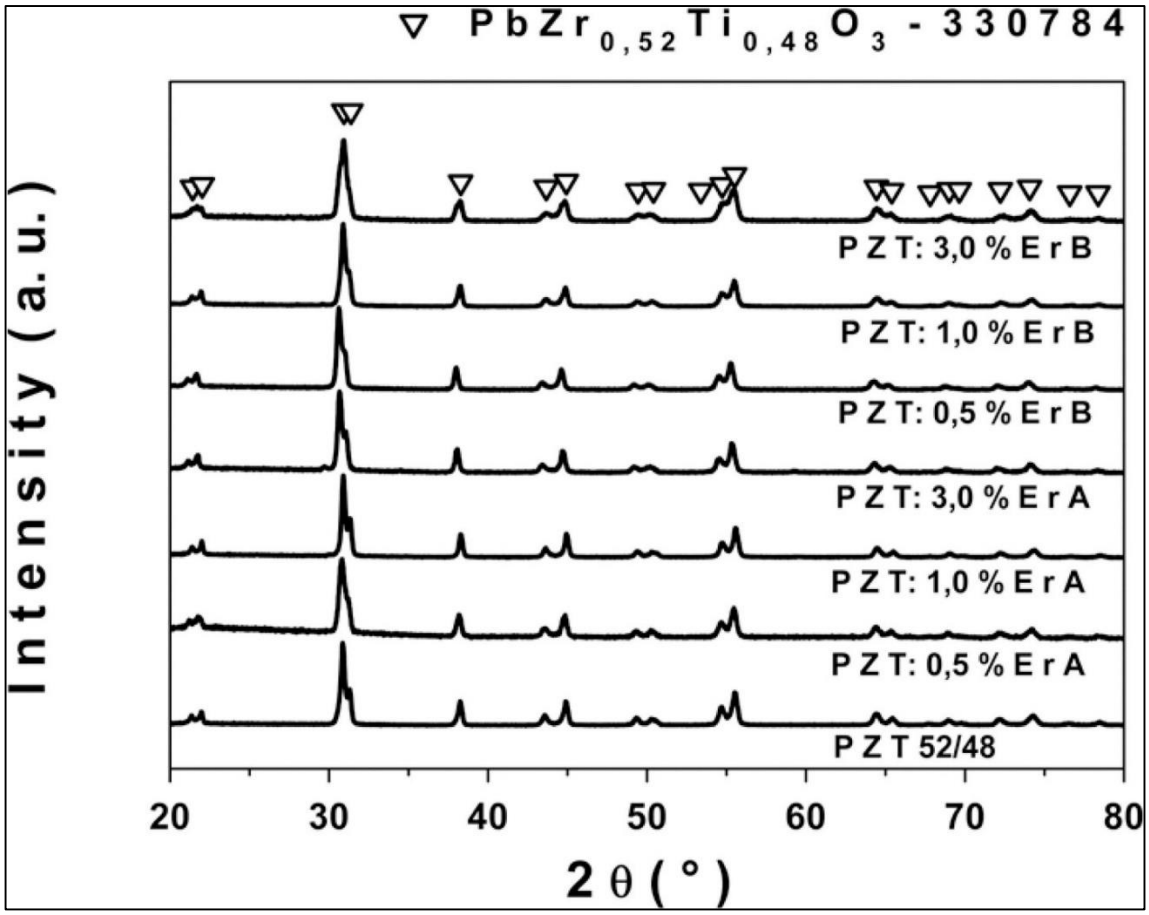

Figure 2-15 XRD patterns of sintered PZT (all compositions) [40].

The residual polarization (P_r) of an undoped PZT sample is 6.99 µC/cm^2 and the coercive field (E_c) is 11.31 kV/cm. P_r and E_c values for doped samples at site A are affected by Er content Figure 2-16. On contrast, the comparable values for doped samples in site B are similar. [40].

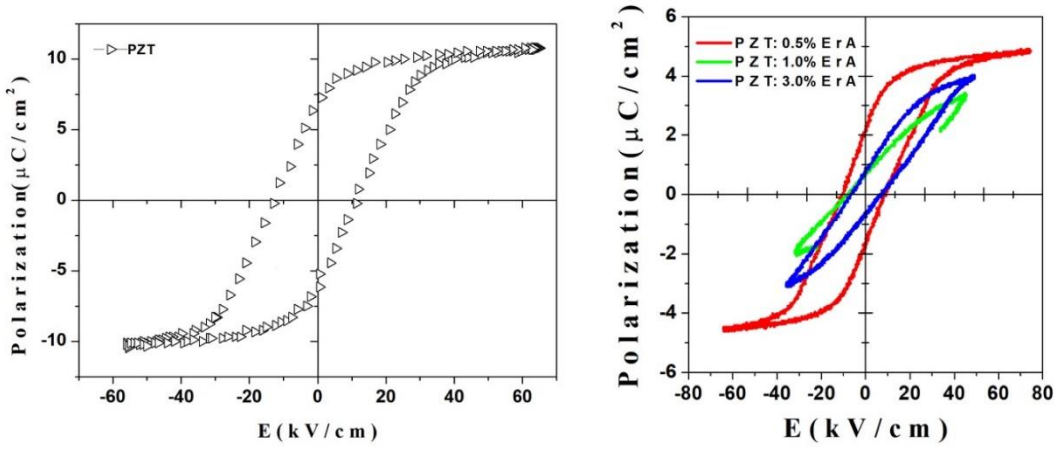

Figure 2-16 Room temperature hysteresis loops for all compositions[40].

Also, Pereira et al. studied the effect of aliovalent Nb doping on microstructural development and electrical properties in PZT (65/35) bulk materials. The XRD analysis of the samples is displayed in the Figure 2-17 It typically shows a consistent distribution of peaks, corresponding to a rhombohedral phase. It should be emphasized that no pyrochlore phase development is visible in any of the spectra up to 7% mol Nb. Figure 2-18 shows the effect of niobium content on density and grain size. After sintering, the final density is high (>92%). In comparison to undoped PZT, densification appears to be more effective as Nb concentration increases. While the particle size remained small, the relative density climbed to 96%. The novel biphasic structure, perovskite and fluorite phases appear to favor grain size formation for Nb > 7%.

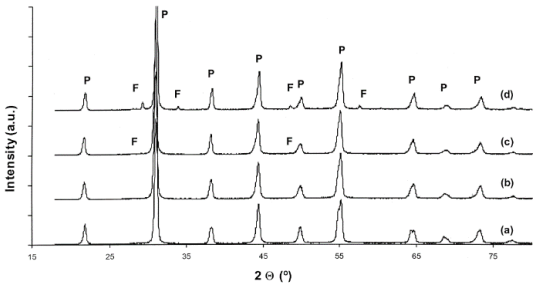

Figure 2-17 PZTN - XRD patterns with varying Nb content: (a) 2% mol; (b) 5% mol; (c) 8% mol; (d) 10% mol; (F, fluorite phase; P, perovskite phase) [41].

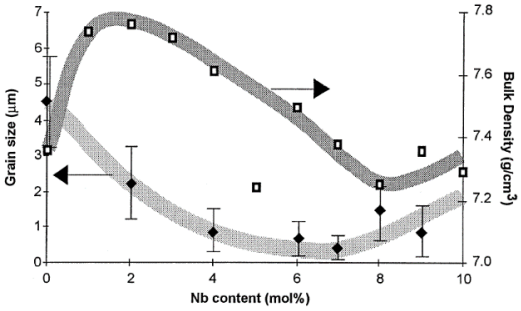

Figure 2-18 density and grain size for certain PZTN compositions vs. Nb concentration[41].

The permittivity and Curie point decreases as niobium concentration increase, and the dielectric constant displays diffuse behavior as a function of temperature rather than a distinct transition. Figure 2-19. P-E hysteresis loops on PZTN (65/35/5) were used to acquire ferroelectric characteristics. This composition, as illustrated in Figure 2-20, has a ferroelectric memory loop with residual polarization of 2µC/cm^2. The loop is more square than PZT (65/35) or PLZT (6/65/35)[41].

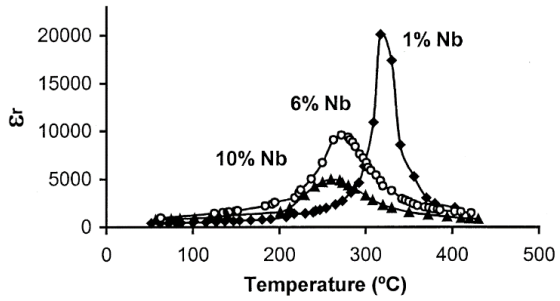

Figure 2-19 Dielectric behavior of several PZTN [41].

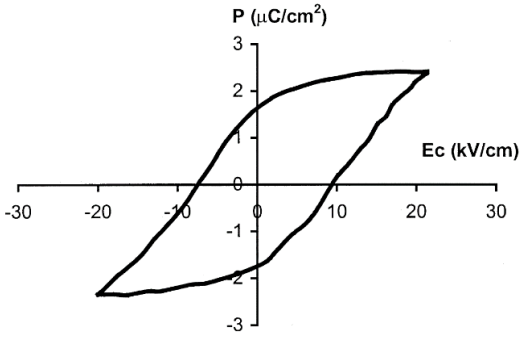

Figure 2-20 Polarization agents electric field hysteresis loop of PZTN (65/35/5) [41].

Another researcher, Sahoo, investigated the impact of La^{3+} and Nd^{3+} on the dielectric, piezoelectric, and ferroelectric characteristics of PZT (Pb ($Zr_{0.53}Ti_{0.47}$) O_3). Figure 2-21. shows XRD patterns of undoped, doped PZT samples. At increasing dopant concentrations up to (0.06 mol), undoped PZT displayed pure tetragonal phase (indicated by tetragonal splitting) and pure rhombohedral phase. The intermediate compositions had a combination of tetragonal and rhombohedral phases, with the tetragonal phase decreasing as the dopant concentration increased.

Figure 2-22 depicts the piezoelectric characteristics of the samples. Doped samples have a considerably greater d33 than undoped PZT samples.

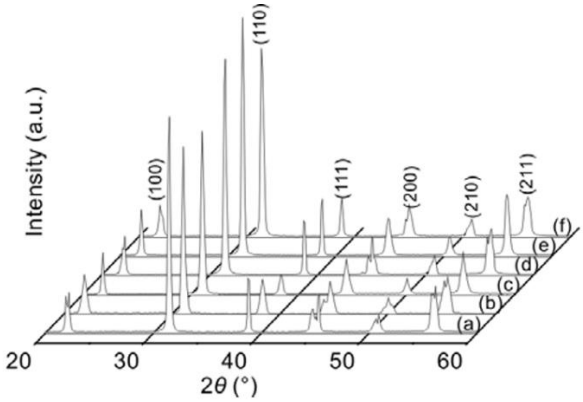

Figure 2-21 XRD patterns of (a) undoped PZT, (b) 0.03 mol La3+ dopants, (c) 0.06 mol La3+ dopants, (d) 0.02 mol Nd3+ dopants, (e) 0.06 mol Nd3+ dopants and (f) 0.01 mol La3++ 0.01 mol Nd3+ doped PZT samples.

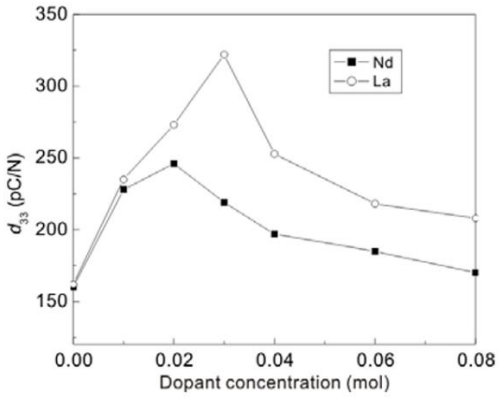

Figure 2-22 Variation in d_{33} with increase in La^{3+} and Nd^{3+} concentration.

Figure 2-23.depicts the samples' P–E hysteresis loops. The undoped sample exhibits considerably low residual and saturation polarization as compared to the doped samples. The greatest residual polarization (*P*r) of a sample containing La^{3+} (0.03 mol) was 18.03 μC/cm2. The residual and saturation polarization in Nd3+doped samples is lower than in La3+doped samples.

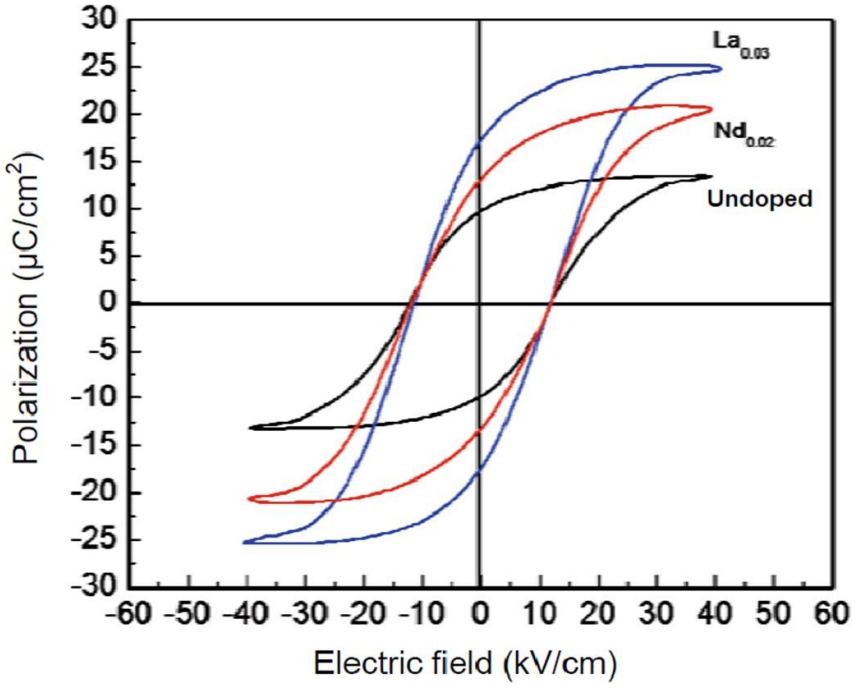

Figure 2-23 Hysteresis loops of undoped, 0.02 mol Nd3+ doped and 0.03 mol La3+ doped PZT sample[42].

Figure 2-24. shows typical SEM images of chemically etched sintered pellets. The grain size reduces when the dopant concentration increases above 0.02 mol Nd^{3+} and 0.03 mol La^{3+}, respectively [42].

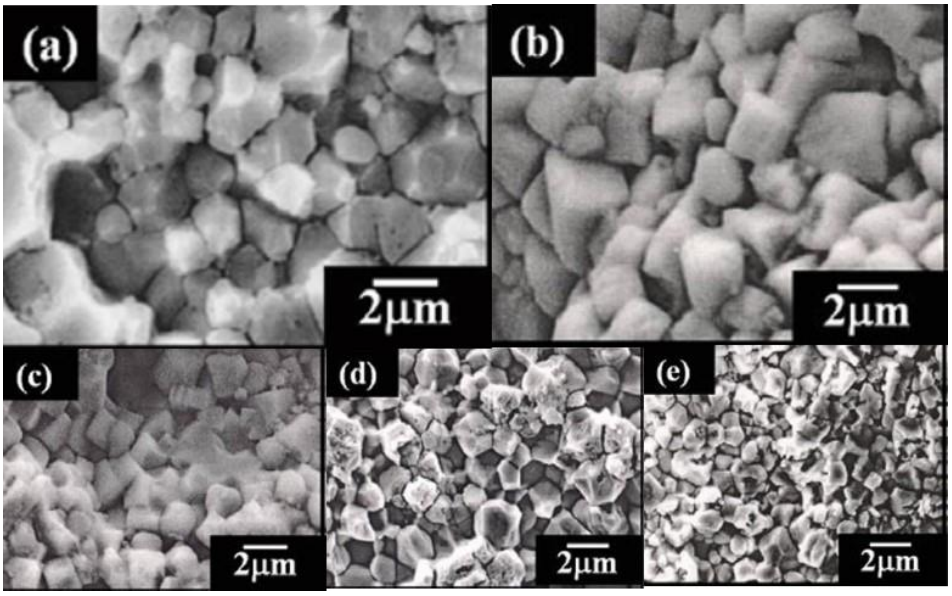

Figure 2-24 SEM images of chemically etched (a) undoped PZT, (b) 0.02 mol Nd^{3+}, (c) 0.06 mol Nd^{3+}, (d) 0.03 mol La^{3+} and (e) 0.06 mol La^{3+} doped PZT sintered pellets. [42].

Finally, Muhammad's thesis was reviewed which studied the effect of La^{3+} on ferroelectric and dielectric properties of PZT. Room temperature XRD patterns of the PLZT ceramics are shown in Figure 2-25, illustrating the effect of La doping on their crystal structure. For example, by comparing the PLZT composition (2/50/50), having tetragonal structure, with the unmodified PZT (50/50) composition, Figure 2-26, it is evident that the tetragonality or the lattice distortion along the tetragonal *c*-axis was decreased after doping[43].

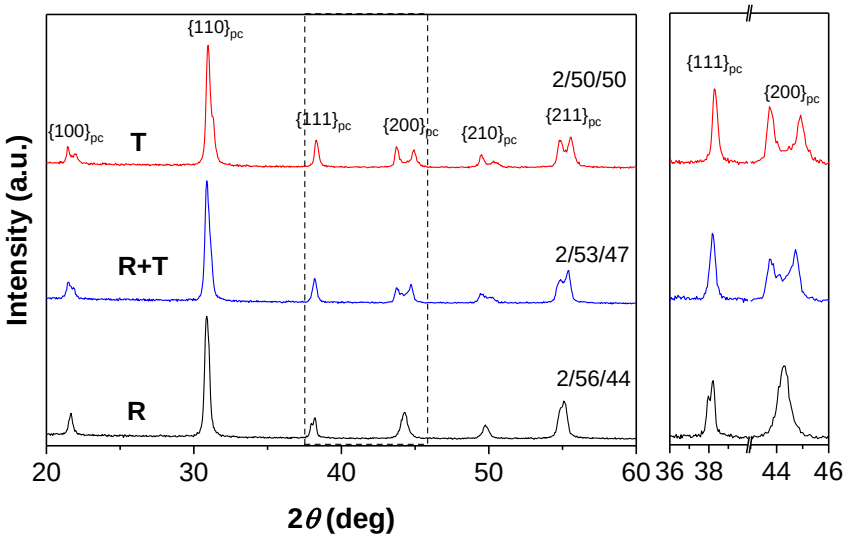

Figure 2-25 XRD patterns for the PLZT ceramics sintered at 1250 ºC for 2 h [43].

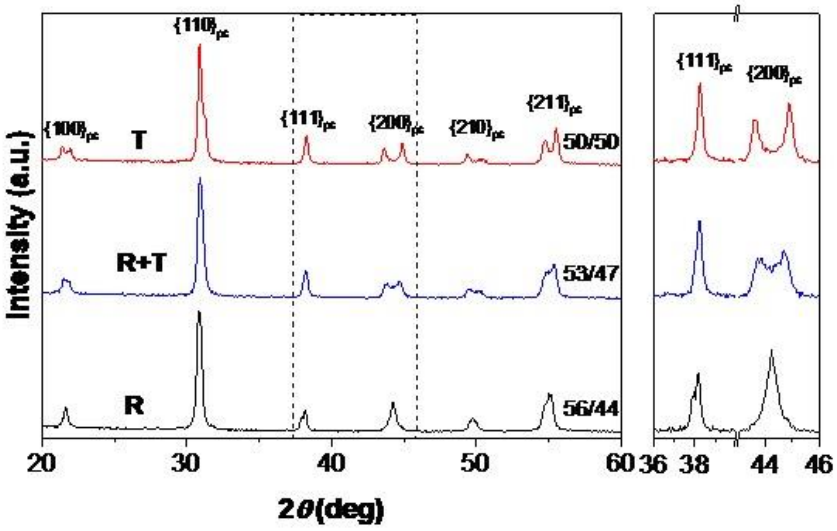

Figure 2-26 XRD patterns for the PZT ceramics sintered at 1250 ºC for 2 h [43].

The effects of La-doping on the ferroelectric P-E hysteresis loops of PZT ceramics at room temperature are illustrated in Figure 2-27. It can be seen that the presence of La has a positive effect, with the remanent polarization (P_r) and coercive field (E_c) being increased significantly[43].

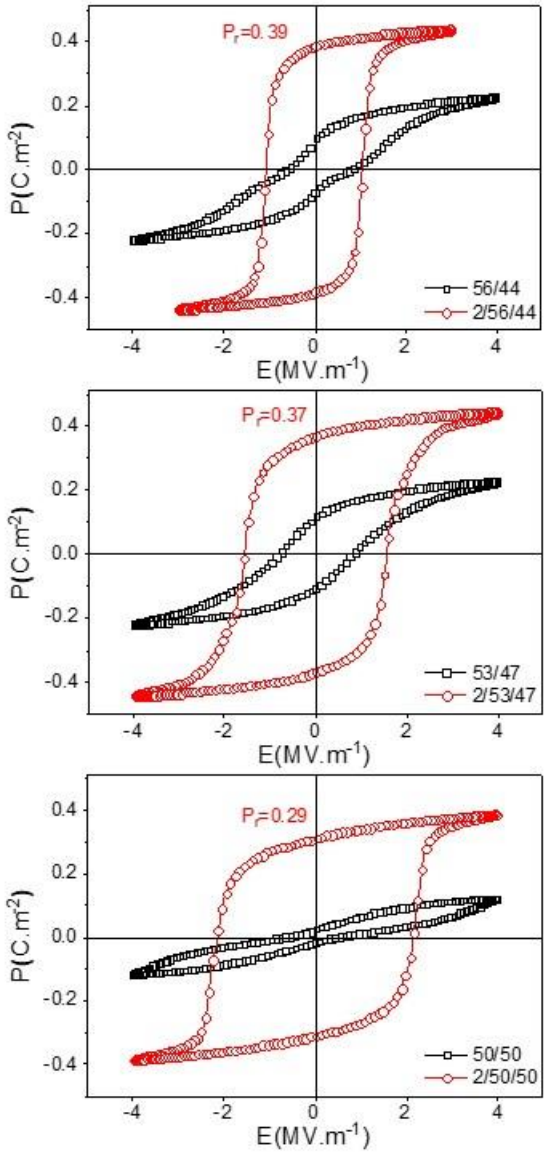

Figure 2-27. P-E hysteresis loop at room temperature for PZT and PLZT ceramics [43].

2.4.1.2 Hard doping

Hard PZT ceramics are created by doping acceptor ions like Na^{+}, K^{+} (for site A) and Fe^{3+}, Al^{3+}, Mn^{3+} (for site B) into the lattice, resulting in oxygen vacancies [12–14]. High electrical and mechanical loads may be applied to hard PZT materials. Their characteristics hardly little change under these conditions, indicating that they are relatively stable. As a result, hard PZT materials are well suited to high-power applications. The moderate permittivity, low dielectric losses of hard PZT ceramics, and large

piezoelectric coupling factors are other benefits, allowing them to be used in resonant mode with little inherent warming. Ultrasonic cleaning, sonar technology, ultrasonic processors, medicinal fields, transformers, and other applications employ piezo components.[39]

Several publications on hard doping were studied. The effect of Fe on lead zirconate titanate ceramics was studied by Sangawar et al. Figure 2-28(a). depicts the XRD peaks of PZTF1, PZTF2, and PZTF3. The XRD patterns obtained show a single perovskite phase for all compositions with no extra peaks, confirming solid solution formation. The amount of tetragonal splitting in PZT rises as the Fe level increases. According to the impact of the Fe dopant concentration on the lattice structure, the SEM microstructure revealed grain sizes of (2.10, 1.22, and 3.20μm) for PZTF1, PZTF2, and PZTF3 samples, respectively Figure 2-28 (b-d). The microstructure of the PZTF2 sample is characterized by regular grain growth, smaller grain size, and homogenous microstructure. These materials are employed in high power low frequency SONAR applications as flextensional transducers.

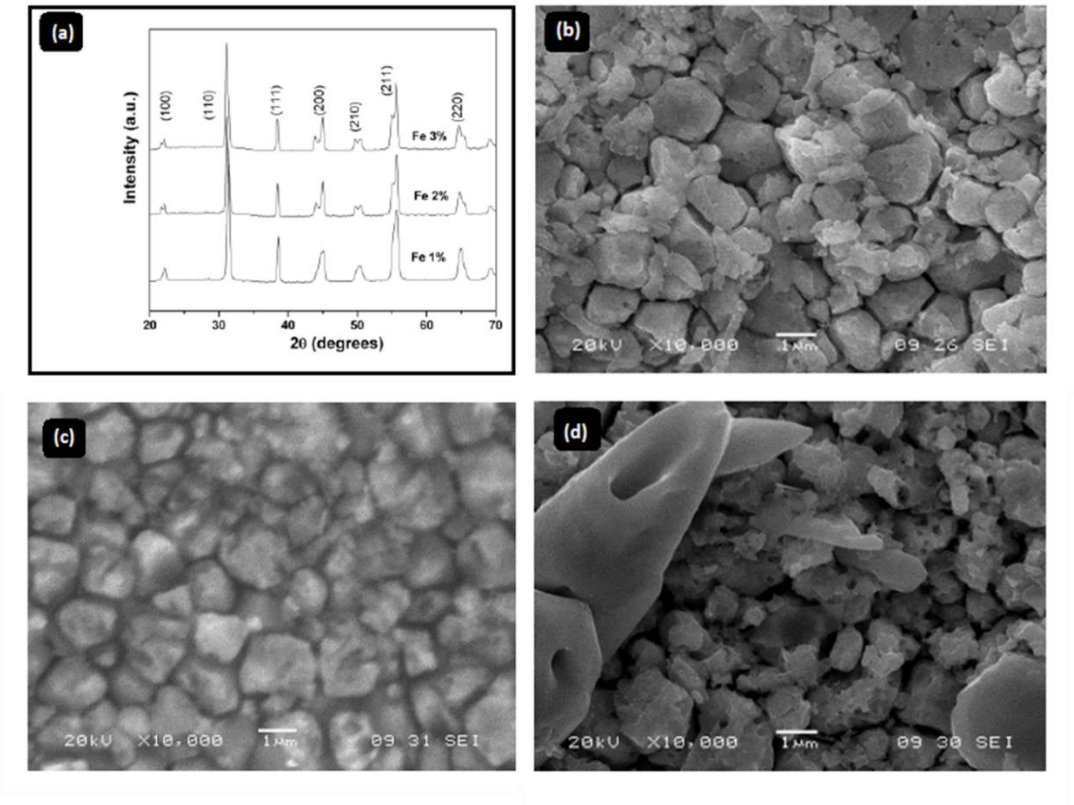

Figure 2-28 (a) XRD of Fe-doped PZT, (b) SEM of the fracture surfaces of Fe doped PZT samples PZTF1, (c) PZTF2 and (d) PZTF3[44].

Figure 2-29 depicts the Dielectric constant variation in Fe-doped PZT samples as a function of sintering temperature. When compared to other PZT samples, PZTF2 samples exhibit a higher dielectric constant (1020) since it possess the smallest grain size [44].

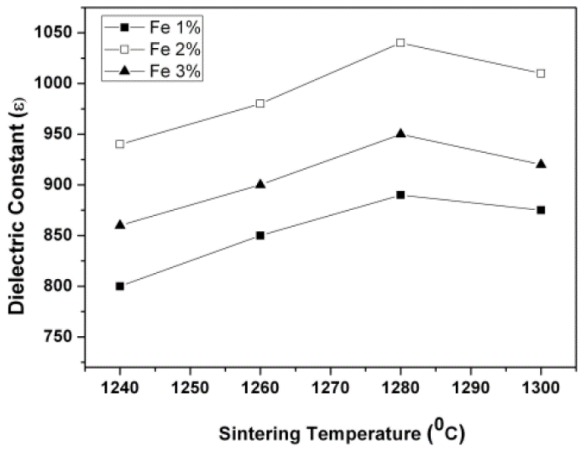

Figure 2-29 Variation of dielectric constant (ε) with Sintering temperature[44].

Also, Mahato, et al. studded the effect of doping lead zirconate titanate (PZT) ceramics with Na^+ dopants. Microstructure of selected samples PZT (unmodified) and 1.5%Na^+ doped PZT (PNZT) sintered at 1100 °C are shown in Figure 2-30. From this figure it is clear that the shape of the grains changes and their size also decreases with incorporation of Na^+ substituents.

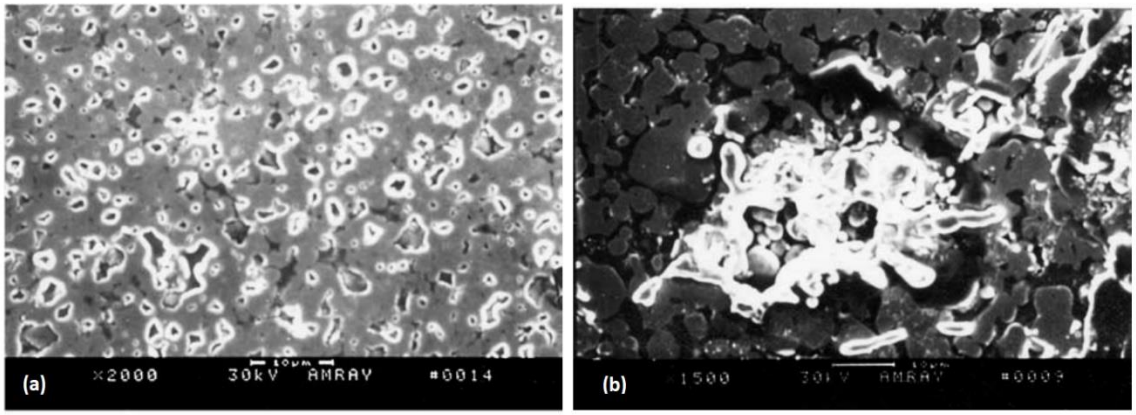

Figure 2-30 Microstructure of (a) PZT and (b) PNZT sintered at 1100 ◦C [45].

It is clear that the Curie temperature of unmodified PZT decreased from 350 ◦C to 250 ◦C after incorporation of 0.5 atomic% Na^+ Figure 2-31. The Curie temperature increases with increase in Na^+ concentration. Curie temperature for 1.5 atomic% Na^+ doped PZT is shifted from 350 ◦C to 280 ◦C and for 2.5 atomic% of Na^+ Tc shifted to 300 ◦C. It is observed that ∈ is decreased by 3.65% for 1.5 atomic% Na^+ doped PZT compared to undoped PZT. The loss tangent (tan δ) of doped PZT is maximum (0.035) at 260 ◦C Figure 2-32. [45]

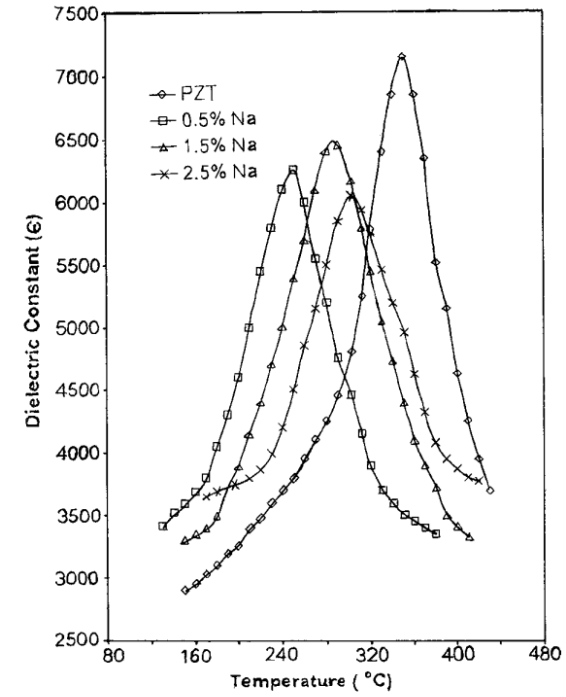

Figure 2-31 Temperature variation of dielectric constant (ε) of PZT and PNZT [45].

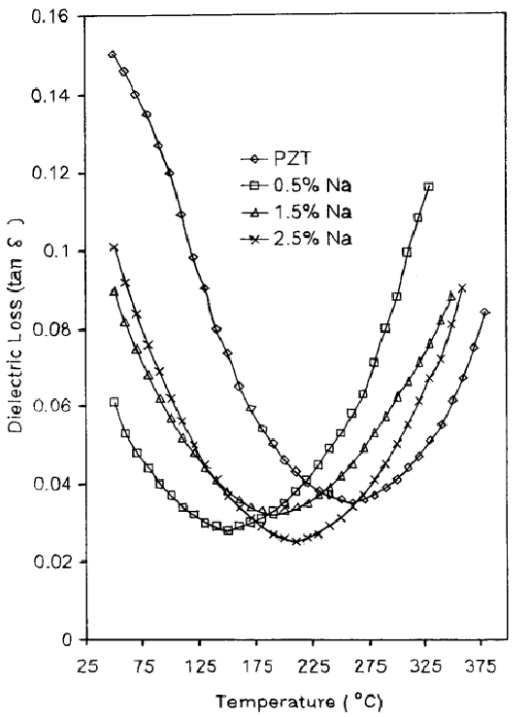

Figure 2-32 Temperature variation of loss tangent (tan δ) of PZT and PNZT[45].

Finally, the effects of Mn/Nb dopant on ferroelectric, dielectric characteristics, phase development, and microstructure, of lead zirconate titanate (PZT) films were studied systematically by Huajun Sun, et al. Figure 2-33 indicated that both Mn- and Nb-doped PZT films had the perovskite structure. It should be noted that the XRD peaks shift to higher angles with increasing Mn doped level. At 100 kHz, the dielectric constant (ϵ_c) and loss tangent (tan δ) were measured. The dielectric constant of 1% Mn-doped PZT films was reduced from 1,320 to around 940, while the loss tangent was enhanced from 0.08 to 0.10. However, when the Mn doping level climbed to 2%, the dielectric constant and loss tangent decreased to 1,100 and 0.08, respectively. Figure 2-34 [46].

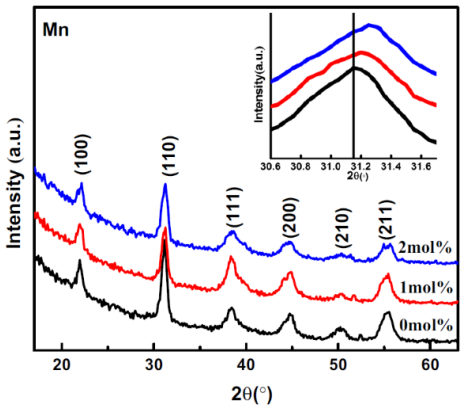

Figure 2-33 XRD patterns of undoped and Mn/Nb-doped PZT 52/48 films and comparison of (110) peaks [46].

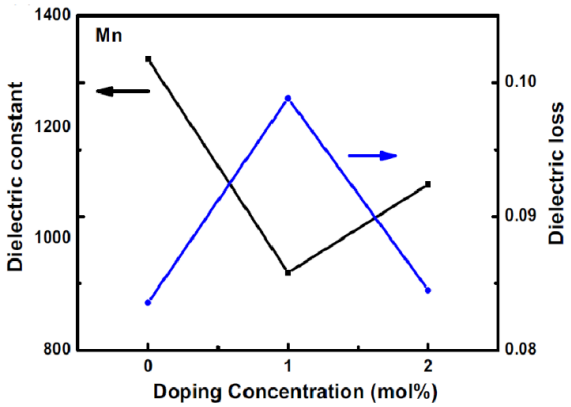

Figure 2-34 Comparison of dielectric properties of PZT and Mn-doped PZT films [46].

2.4.1.3 Isovalent additives

These are divalent cations (e.g. Sr2+) that will substitute Pb2+ on the A site or tetravalent ions (e.g. Sn4+) that will substitute Ti/Zr4+ on the B site.

2.4.1.4 Co-doping

Doping with two kinds of ions, named co-doping, is another form of tailoring ferroelectric properties via partial subibstitution of A-site, B-site or both [47] .

Recently, Bhattarai et al, studied the influence of La^{3+} and Sc^{3+} content on dielectric properties, structural, and ferroelectric of lead zirconate titanate ceramics for energy storage capacitors , as a complex doping, with the stoichiometric formula $(PbZr_{0.53}Ti_{0.47})_{0.90}$ $(La_xSc_{1-x})_{0.10}O_3$ for x = 0.2, 0.4, 0.6, and 0.8.

The higher the concentration of La^{3+} in the composition, the more relaxory the behavior. The P–E loop measurements in specimen with composition at x=8 show that there is an enhanced P_m–P_r, which results in a reclaimable energy density, U_{re} ~ 1162 J/ cm^3 with an efficiency η of ~79% under an applied electric field of ~97 kV/cm, and thus it could be a good option for energy-storage applications.

Figure 2-35 For all compositions, depicts the known room-temperature polarization electric field (P–E) loops. The coercive field (E_c) was observed to decrease as La^{3+} concentration increased. The maximum field Ec was reported for low La^{3+} PLZTS2 and PLZTS4 concentration.

This is consistent with a research on Sc^{3+} doped $PbZr_{0.53}Ti_{0.47}O_3$, in which no significant drop in E_c was seen. [48]. They also discovered that when the lanthanum concentration increases, the spontaneous polarization (Pm) initially increases and subsequently declines the peaks in composition with x= 6 Pm ~ 35 μC/cm^2. The observed narrow hysteresis loop and more changes in the P_m–P_r value for the sample with composition at x=8 indicate that this composition is relaxor in nature[49].

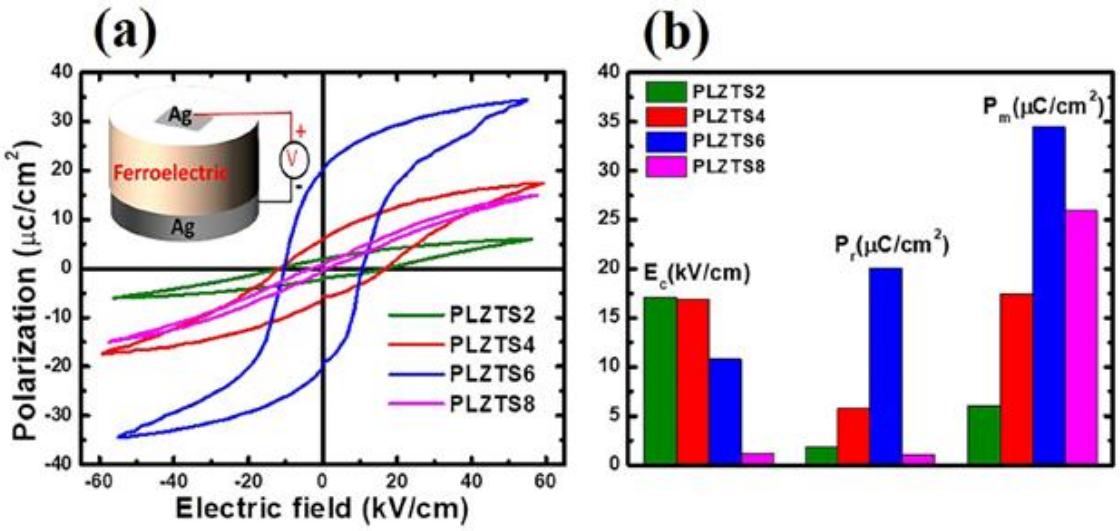

Figure 2-35 (a) Ceramic P–E hysteresis loops at 50 (b) the appropriate E_c, P_r, and P_m values [49].

In addition, Zak, A., et al. investigated the influence of Y^{3+} and Nb^{5+} co-doping on the piezoelectric and dielectric characteristics of PZT ceramics. According to the XRD results, shows the presence of a two-phases of perovskite, rhombohedral and tetragonal phase and free from pyrochlore phase. Tetragonality rises at doping levels x = 0.01 and x = 0.03, as seen by the appearance of a new peak next to the previous peak at 2 θ = 73°. Figure 2-36

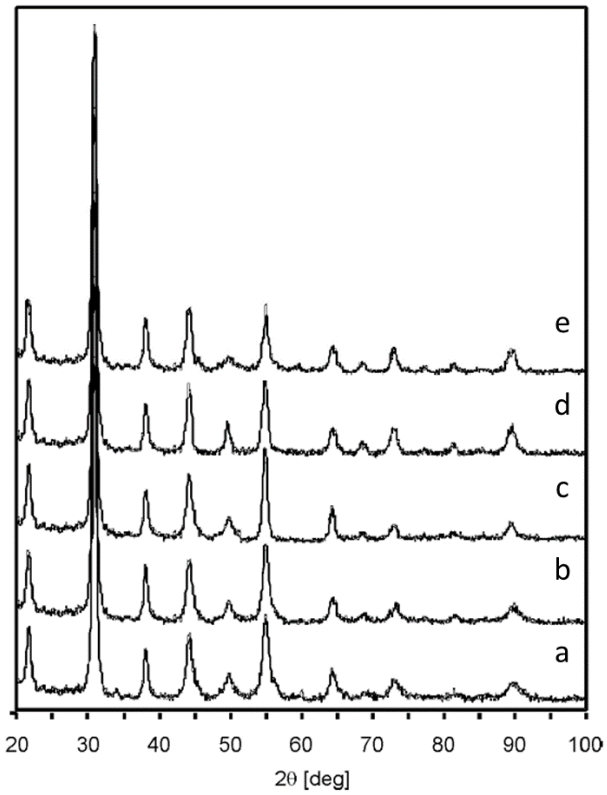

Figure 2-36 XRD patterns of $Pb_{1-x}Y_x(Zr_{0.53}Ti_{0.47})_{1-x}Nb_xO_3$ samples: a) x = 0.0, b) x = 0.01, c) x = 0.015, d) x = 0.02, and (e) x = 0.03

Figure 2-37 and Figure 2-38 show SEM images of doped and undoped PZT with Y and Nb (x = 0.015). The SEM results show that the average grain size of doped PZT is around 3μm, which is smaller than that of pure PZT.

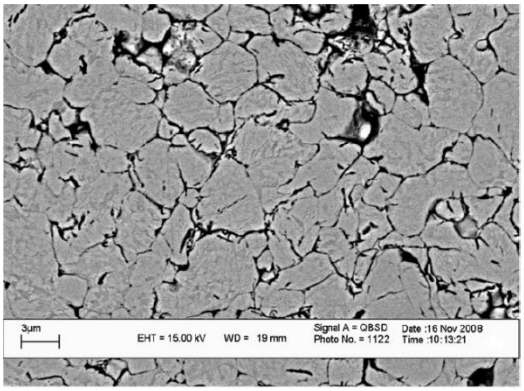

Figure 2-37 Typical SEM images of pure PZT ceramics (Zr/Ti ratio 53/47) [50].

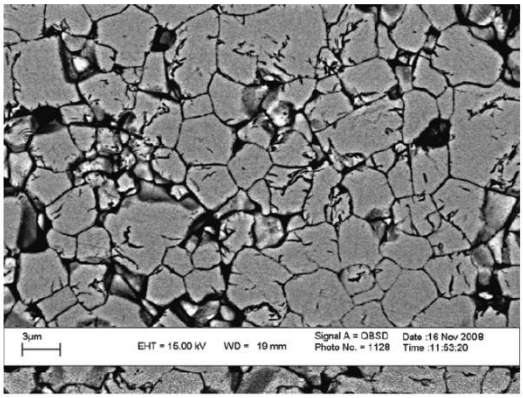

Figure 2-38 Typical SEM image of doped PZT (x = 0.015) ceramics (Zr/Ti ratio 53/47) [50].

The samples' electric permittivities increase to (945 at x = 0.02) after co-doping with Nb and Y. Doped PZT ceramic densities initially grow in proportion to doping level. At x = 0.010, maximum density is reached; as x grows, density becomes inversely proportional to doping level.[50]

2.4.2 Applications.

Piezoelectric ceramics are very hard, chemically inert, and resistant to humidity and other environmental factors. Their mechanical characteristics are similar to that of more well-known ceramic insulators, and they are made using similar techniques. All forms of electromechanical transducers benefit from piezoelectric components. Piezoelectric components are appropriate for all forms of electromechanical transducers. [51]. Here are just a few of the various applications where our PZT materials may be found.

1. It used in Generators (conversion of mechanical into electrical energy)
   - solid-state batteries
   - spark igniters
2. Sonic and ultrasonic transducers (conversion of electrical into mechanical energy)
3. Sensors (Converting a mechanical force into an electrical signal)
   - pressure sensor
   - knock sensor (internal-combustion engines)
   - acceleration sensor

2.5 Synthesis Routes for PZT Powders

Mixed-oxide ceramic powders have been synthesized using a number of techniques. These techniques are now available for both laboratory and industrial use. PZT powders have been made using the majority of them [52]. A broad comparison of oxide ceramic powder production methods is as follows:

1. solid-state reaction
2. sol-gel
3. coprecipitation
4. spray pyrolysis
5. hydrothermal synthesis
6. emulsion synthesis

2.5.1 Solid-State Reaction

The rate of densification, as well as the rate of solid-state response, of multicomponent powders, is strongly influenced by the average particle size, with the finer the average particle size, the greater the sintering and chemical reaction rates for most ceramic materials. Powder milling or comminution is commonly required to produce chemically homogenous, finely split powders with a desired particle size distribution and little or no particle aggregation. For size reduction of raw materials selected for the production of numerous ceramics, a range of crushing and grinding equipment is used. Vibratory mills, centrifugal mills, colloid mills, ball mills, and fluid energy mills are some of the mills used in the ceramic industry for fine grinding operations[53].

PZT powders are typically made via one-stage solid-state reactions in a combination of PbO, TiO_2, and ZrO_2Oxides. During calcination, there are four areas that correspond to four chemical processes.[54] Figure 2-39, i.e.

Zone I: no reaction (Temp.<350°C);

Zone II: $PbO + TiO_2 \rightarrow PbTiO_3$ (350°C <Temp.< 700°C);

Zone III: $PbTiO_3 + PbO + ZrO_2 \rightarrow Pb(Zr_{1-x}Ti_x)O_3$ (650°C<Temp.<800°C);

Zone IV: $Pb(Zr_{1-x}Ti_x)O_3 + PbTiO_3 \rightarrow Pb(Zr_{1-x'}Ti_{x'})O_3$ (x<x') (800°C<Temp.<1000°C).

The calcining technique in industrial production usually entails keeping the product at temperature of 650°C for one to two hours after that it keep at 850°C for two hours.

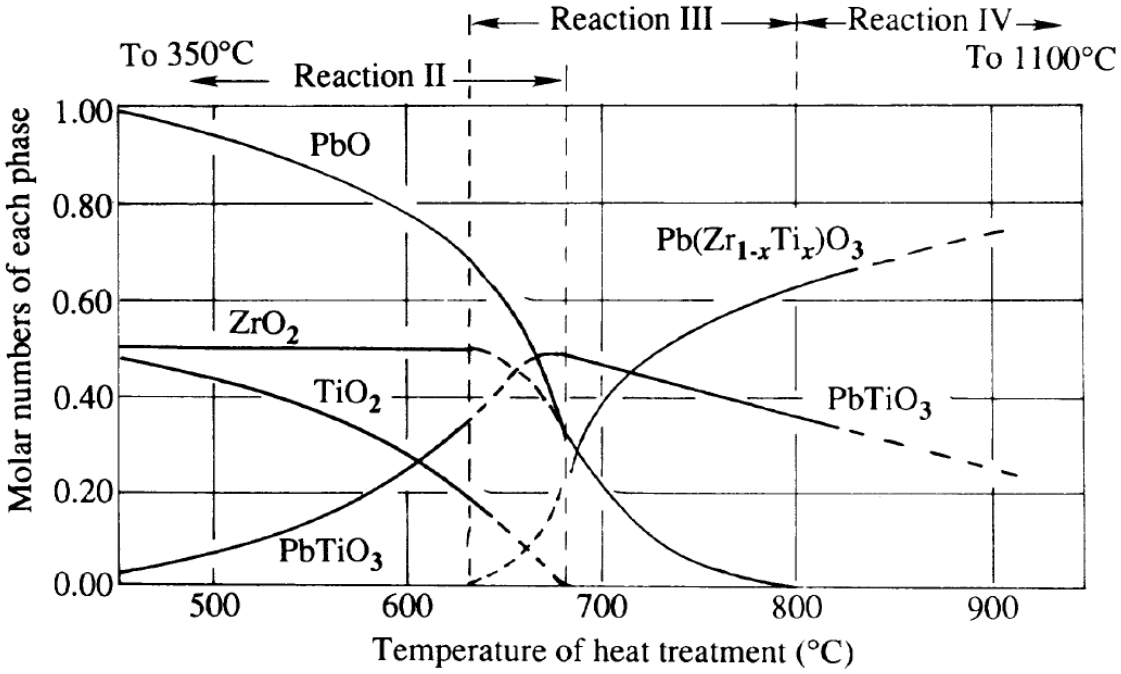

Figure 2-39 Solid state reactions with increases of calcination temperatures[54].

As illustrated in Figure 2-39, the reaction mechanism of the classic one-stage solid-state reaction leading to PZT solid-solution production really requires many phases, PbTiO3 (denoted as PT) is formed early in the reaction, followed by the creation of certain intermediary phases.[55]

2.5.2 Sol- gel

The sol-gel technique Figure 2-40 depicts the formation of a heterogeneous gel from liquids followed by drying at low temperatures. Because gel formation begins with a solution of all components in the form of soluble precursor chemicals, molecular mixing is maintained. The most advantageous aspects of this technique are its high purity and full control over the composition of the resulting powders. Partially hydrolyzed metal alkoxides or salts result in crosslinking and branching. This polymerization

procedure creates 3D structures while avoiding segregation. The hard coherent gel is subsequently dried and heated at much lower temperatures than in previous procedures[56].

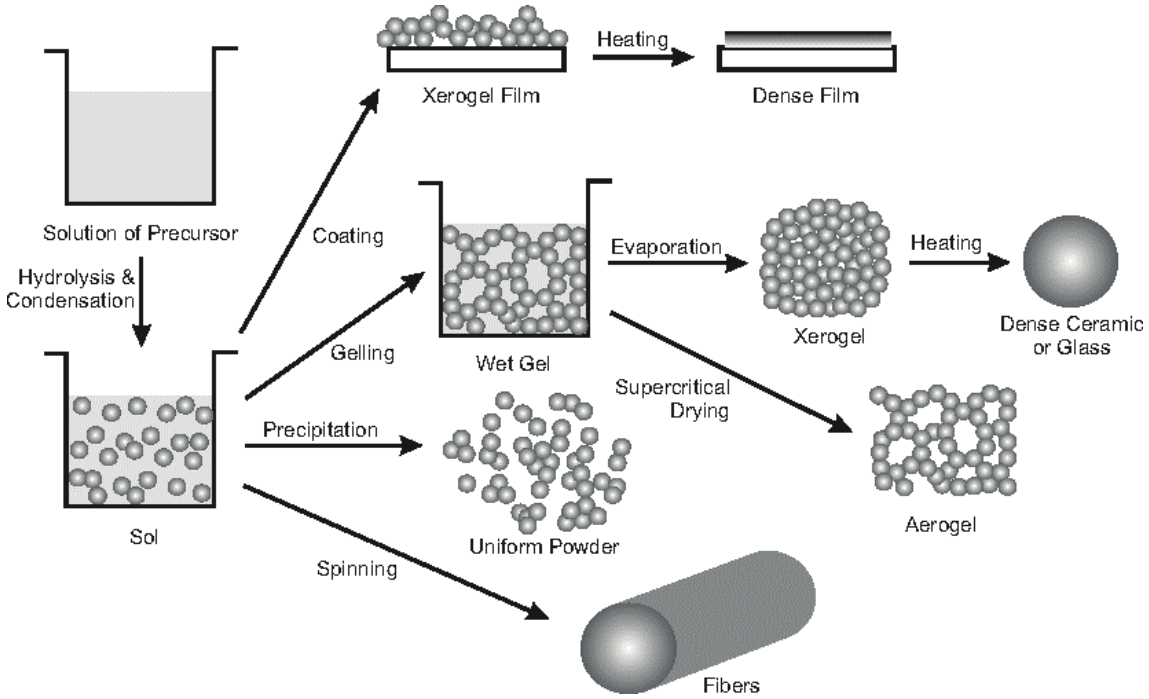

Figure 2-40 The sol-gel process [56].

Chapter Three

Experimental procedures

3 Experimental procedure

This chapter covers the synthesis of PZT, PLZT, PSZT, and PL-SZT powders, as well as the processing of ceramics. The sample preparation processes, conditions, and characterization techniques are all described in detail the microstructure and electrical characteristics of the samples are also reported as shown in Figure 3-1.

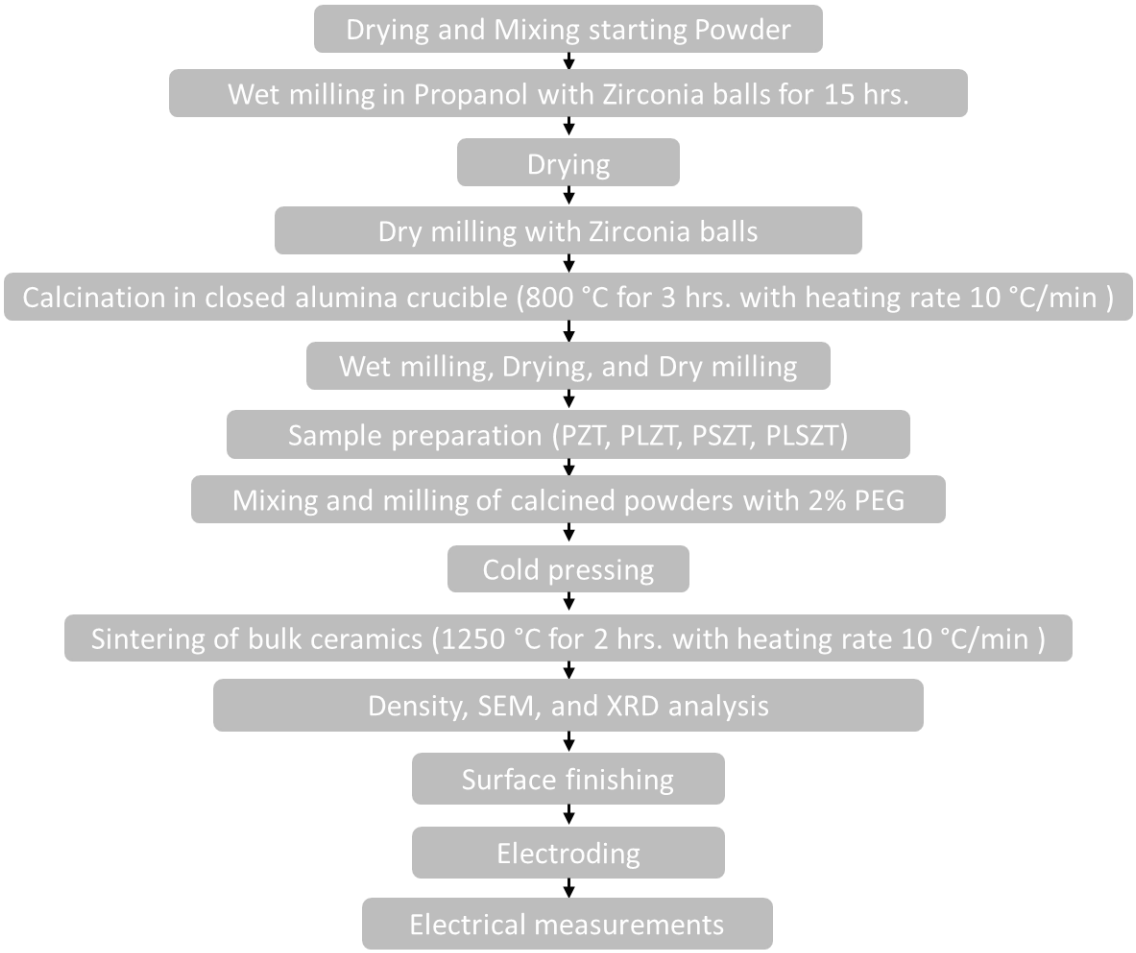

Figure 3-1. The samples preparation processes

3.1 Composition selection

The doping in PZT composition close to MPB region could help to cause a phase transformation which can be employed in different applications, where the MPB is approached consequently the dielectric and piezoelectric properties are considerably enhanced. In this regards, PZT composition at

Zr/Ti ratio equil to 0.56/0.44] was chosen based on the formula Pb (Zr_{1-x} Ti_x)O_3 which is located at rhombhedral region. The dopants ions La^{+3} and Sc^{+3} will substitute the Pb^{+2} and Zr^{+4} sites, respectively[7].

The composition was doped with 2% Lanthanum ($La^{3+)}$ as a donor dopant at the A-site ($Pb_{0.98}$ $La_{0.02}$) ($Zr_{0.56}Ti_{0.44}$) O_3 [PLZT] and 2% Scandium (Sc^{3+}) as an acceptor dopant at the B-site Pb ($Sc_{0.02}$ $Zr_{0.54}$ $Ti_{0.44}$) O_3 [PSZT]. Furthermore, co-doping with 2% Lanthanum and Scandium ($Pb_{0.98}$ $La_{0.02}$) ($Sc_{0.02}$ $Zr_{0.54}$ $Ti_{0.44}$) O_3 [PL-SZT]. Table 3-1 summaries the selected composition in addition to the other doped.

Table 3-1 Undoped and doped PZT compositions

Doping status	Abbreviation	Stoichiometric formula
Undoped PZT ceramic	PZT	Pb ($Zr_{0.56}$ $Ti_{0.44}$) O_3
Soft PZT ceramic La donor at A-Site	PLZT	($Pb_{0.98}$ $La_{0.02}$) ($Zr_{0.56}$ $Ti_{0.44}$) O_3
Hard PZT ceramic Sc acceptor at B-Site	PSZT	Pb ($Sc_{0.02}$ $Zr_{0.54}$ $Ti_{0.44}$) O_3
Co-doping La donor at A-Site Sc acceptor at B-Site	PLSZT	($Pb_{0.98}$ $La_{0.02}$) ($Sc_{0.02}$ $Zr_{0.54}$ $Ti_{0.44}$) O_3

3.2 Synthesis of PZT- Powder

To make pure and doped PZT, high purity powders of PbO (Sigma Aldrich 99% purity), La_2O_3 (Alfa Aesar 99.9% purity), ZrO_2 (Magnesium Elektron E-101), TiO_2 (Huntersman A-HR 99% purity), and Sc_2O_3 were used. powders of PZT, PLZT, PSZT, and PL-SZT ceramic were prepared using the solid-state reaction method.

Starting powders were weighed according to the molar ratios of the chosen composition, with an excess of 0.03 mol. percent PbO added. Inside

polyethylene bottles, they were wet-milled using Isopropanol and zirconia balls (7.0 mm in diameter) as milling media. The mixture is then placed in a roller-milling machine for 15 hours. 20 g powder, 25 ml Isopropanol, and 20 g medium were used in a typical mill. The slurry is then dried at 90 °C. A high-density alumina crucible with an alumina plate was used to calcine dry particles. The powders were calcined for three hours at 800 °C, rate of heating 10 °C/min. Calcined powders were wet milled for 15 hours in a manner similar to the original milling to promote agglomeration size reduction. [57]

3.3 Bulk sample preparation.

To increase the plasticity of the powders, a 2% wt. of (PEG) (Polyethylene glycol) was utilized as a binder in a water solution to form pellets as samples for various tests. Powders and PEG solutions were combined, dried, and then milled using zirconia balls in a roller milling machine. The dry powder, including the binder, was pressed uniaxially into pellets in cylindrical stainless-steel dies for 30 seconds at a pressure of 12 Kg/ cm^2. These pellets were (10 mm) in diameter and (0.9 to 1.2 mm) in thickness, dependent on the electrical measurement's requirements. To prevent severe evaporation of the lead during sintering, pellets were put on a thin layer of zirconia sand (baddeleyite sand) and covered with an alumina crucible in the presence of $PbZrO_3$ powder. Sintering was conducted in steps. First, heat samples to (500 $^{\circ}$C), rate of heating 5°C/min and soak for 30 min. to guarantee complete binder removal. After that, the bath was burned in 1250 °C at a rate of heating 10 °C/min and kept for 2 hours as a dwell period [57].

3.4 Electroding.

The surfaces of sintered samples were ground to achieve parallel sides for electrical tests using P 800, P 1000 and P 2000 SiC sheets. The electrodes were then painted with silver paint. To ensure that the electrode layer is thin

and consistent, silver paint diluent was used to thin the silver pastedown to the desired viscosity level. After painting, each face was dried for 20 minutes in an oven at roughly 85°C. Following this first drying, the samples were heat-treated for one hour at 550°C to ensure that the electrodes and ceramic surfaces were in touch. The organic compounds employed in the silver paste had to be removed, therefore this high-temperature burning was required. Furthermore, this heat-treatment reduced residual surface tensions caused by grinding [58].

3.5 Basic characterization.

3.5.1 Phase identification.

XRD (SHIMADZU XRD 6000), which located in the laboratories of ceramic engineering and building materials department) with CuKa radiation was used to conduct crystallographic and phase analyses on calcined powders and sintered samples as a powder form with a 0.02° step size and a speed of 6°/min, the detection range was 20 to 60 degrees. The peak positions of the data were compared to the information from the JCPDS standards in order to determine the presence of the perovskite structure and phases.

3.5.2 Microstructure analysis

The microstructural features such as grain size, grain boundary, and pores of sintered samples were characterised by scanning electron microscopy (VECA3 TESCAN, located in the laboratories of ceramic engineering and building materials department).

The sintered samples grinded using P 800, P 1000 and P 2000 SiC sheets and polished using cloth with polishing paste 6 µm, 1 µm and 0.25 µm. Chemical etching process was used to reveal grain boundaries. Etching

solution that was used: 4% HCl +1% HF+ 95% distill water. The samples were etched for 20 seconds with an immediate washing under running water. Then, the microstructures were checked under an optical microscope [58]. Afterwards samples were fixed to an aluminium stub using double sided copper adhesive tape. Finally, Au coated samples for 40 sec before the SEM observation[57].

3.5.3 Density measurement.

The density was calculated from the masses and dimensions of the ceramic samples to obtain an indication of densification process.

3.5.4 Dielectric properties determination.

The dielectric properties of the sintered samples were studied as functions of frequency. LCR meter is used to measure dielectric loss and capacitance. In an automated LCR meter bridge approach, the bridge circuit consists of a fixed standard resistance next to the unknown resistance and a multiplying digital to analog converter (MDAC) that acts as a resistive potentiometer. [57]. The Agilent impedance analyzer is an American-made LCR meter with a frequency range of 50Hz-5MHz, as indicated in the diagram. Figure 3-2.

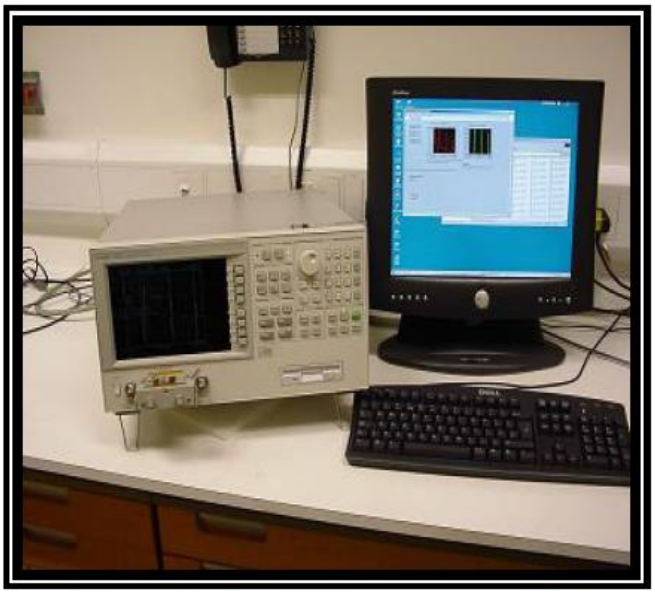

Figure 3-2 LCR Meter

The capacitance (C_p) and the dielectric loss tangent (tan δ) or (dissipation factor) are determined. These measurements were performed at frequencies up to 1 MHz).

The dielectric constant (ε_r) of a material can be determined from the capacitance (C_p) according to equation (3-1).

$$\varepsilon r = \frac{Cp\ d}{A\ \varepsilon o} \quad (3\text{-}1)$$

Where:

ε_r: the dielectric constant of the piezoelectric material.

Cp: the capacitance of the sample.

d: the thickness.

A: the surface area of the PZT sample.

ε_o: Permittivity in vacuum, note that $\varepsilon_o = 8.854 \times 10^{-12}$ F/m.

3.5.5 Dielectric Strength

The samples' dielectric strength was measured at the University of Technology/Department of Applied Sciences, using a (BAUR-PGO-S-3) device up to the voltage (300 kV), as shown in Figure 3-3. Applied electrical field was 60 kV (0.5 kV / Sec), and thickness of the samples was less than 2 mm. The equipment contains the poles of copper which be in contact with the sample, and contains a tub filled with oil, which conducted preliminary testing of the process. It was found that the rate of electricity is the durability (35 kV / mm) for one minute, which is suitable for this purpose, and there is another reason to use the liquid, is high temperature in using (frequency) therefore; make it serve because it acts as inert media, which may get burned by the spark generated

Figure 3-3 Dielectric Strength Instrument

It will be interesting to know that the preferred measure of the breakdown voltage be in many areas for a single sample, and its rate is the best of these measurements due to differences in the homogeneity of the sample, which may occur during the thermal process and the emerging material multi-phases [52,68].

Dielectric strength = $\frac{V_{av}}{h}$ ----------(3-10)

Where:

V_{av}: the rate of breakdown voltage (Kv)

h: thickness (mm)

3.5.6 Dielectric Strength Instrument

The dielectric strength instrument is composed of the following components:

1- A high-voltage provider has used a German-made type (BAUR PGO S3) with a frequency of (50 Hz) and (0-60 kV) voltage range.
2- To avoid the spread of a circumstantial spark (Flashover), as well as to increase the speed of liquid inflammation, The instrument contains a high dielectric strength liquid (voltage transformer oil (40 kV/mm)), and the oil must be replaced to prevent ionization of the liquid, which causes measurement error.
3- As indicated in the illustration Figure 3-3, the instrument has copper rods with strong electrical conductivity and a spherical form of around 2 mm in diameter.

Chapter Four

Results and Discussion

4 Results and Discussion

In this chapter, the results obtained from the prepared and measured undoped and doped PZT ceramics will be discussed in terms of effect of dopants on microstructure, structure, and electrical properties of PZT ceramic.

4.1 Structure and microstructure properties

4.1.1 Structure characterisation

The XRD patterns at room temperature for sintered undoped and doped PZT are shown in the below figures. Generally, peaks are getting sharper (in comparison with that of calcined powder) in agreement with a better crystallization or compositional homogenization due to high temperatures. No peaks associated with second phases are observed.

For the undoped composition, Figure 4-1, the single (200) as well as the little split (111) peaks indicate that the ceramic characterize by rhombohedral structure, which is consistent with previous reports [43]

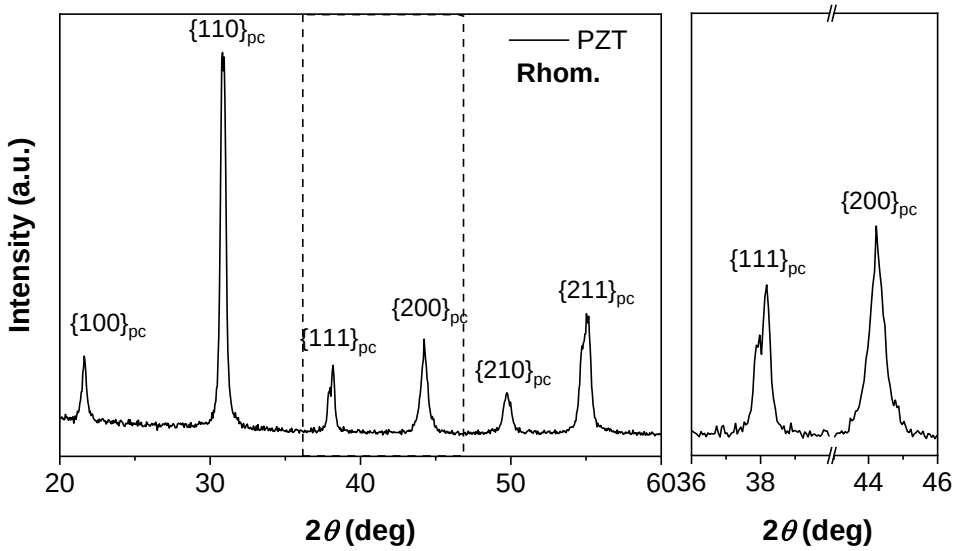

Figure 4-1 XRD patterns for the PZT ceramics sintered at 1250 ºC for 2 h (undoped)

For soft ceramic, labeled PLZT, the influence of incorporation 2% mole of lanthanum on the crystal structure of PZT is illustrated in Figure 4-2. It is

evident that there is no pronounce effect, albeit it can be seen a broadening in the (200) peak.

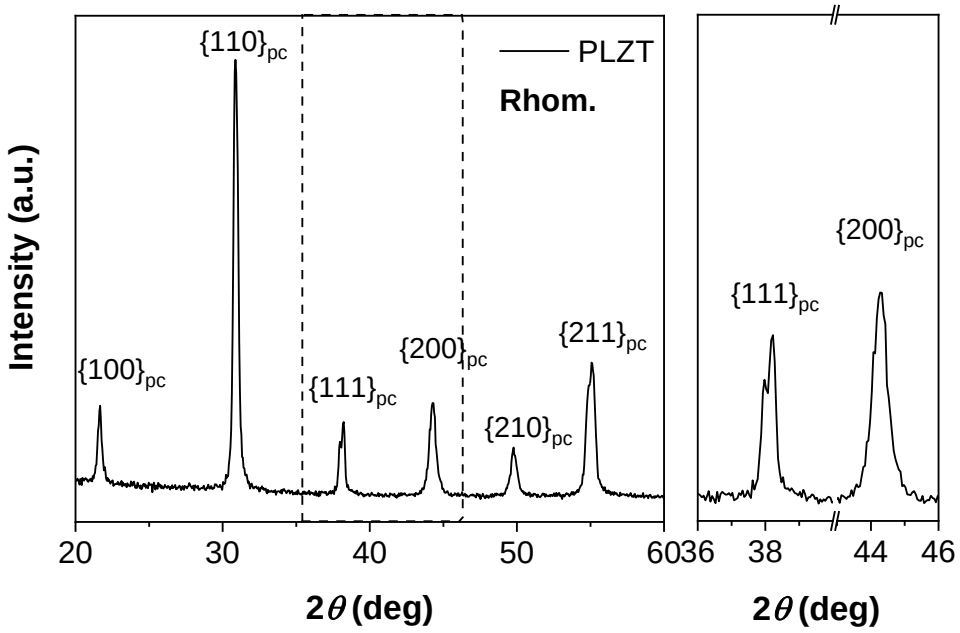

Figure 4-2 XRD patterns for the PLZT ceramics sintered at 1250 ºC for 2 h.

On the other hand, Figure 4-3 clearly shows the XRD pattern of hard PSZT that represented by incorporation 2% mole of scandium at B-Site (on the account of Zr ratio). Apparently, the addition of Sc^{+3} induced partial phase transformation which results in appearance of tetragonal phase beside the rhombohedral phase. This can be well distinguished from the scanning patterns at around $2\theta \sim 44^{o}$, where two overlapping diffraction peaks at the shoulders of (200) peak were observed. These can be ascribed to the development of tetragonal phase. However, the relatively small peak splitting in those planes and splitting of (111) peak indicates a high fraction of the rhombohedral phase. As result, this created coexistence phase region (i.e MPB region) which is consistent with the fact that the compositions are near the MPB.

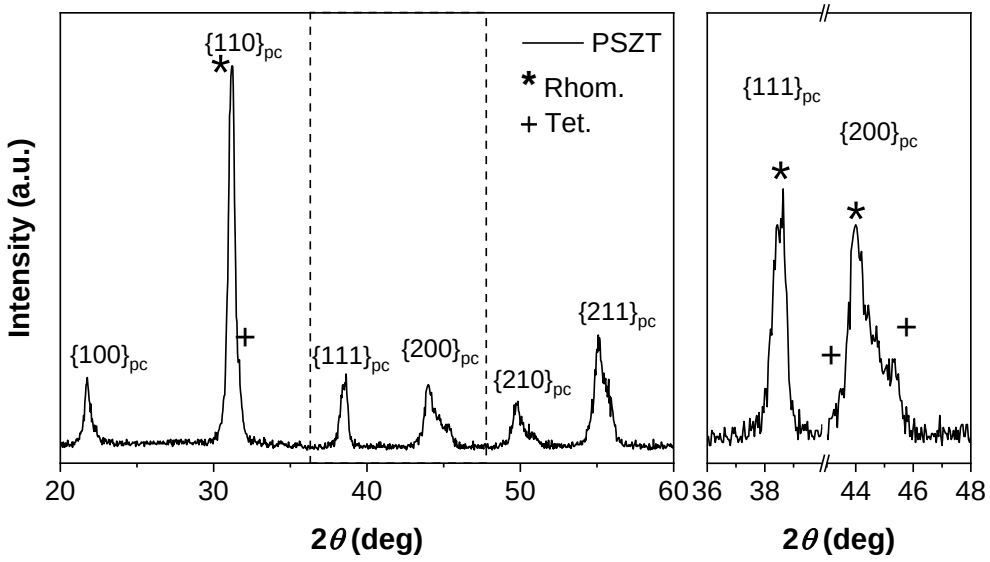

Figure 4-3 XRD patterns for the PSZT ceramics sintered at 1250 ºC for 2 h.

Figure 4-4 show the effect of complex doping on the structure of PZT. In which, 2% mole of both La^{+3} and Sc^{+3} are incorporated at A- and B- site, respectively. Clearly, it can be noticed strong peak splittings in the (200) planes, which suggest increasing of ferroelectric tetragonal phase in comparison with hard PZT (PSZT). Furthermore, with the presence of La^{+3}, it is evident that the tetragonality or the lattice distortion along the tetragonal *c*-axis was decreased after doping, as evidenced by changes in the locations of the $(200)_{pc}$ or $(002)_{pc}$ diffraction peak. This is directly related to the spontaneous strain (i.e the c/a ratio is reduced for the La-doped PZT). This is attributed to the differences in ionic size of Pb^{2+} and La^{3+}, which are 1.20 and 1.15 Å, respectively, and to the less distorted bonding arrangement of the La^{3+} ions.

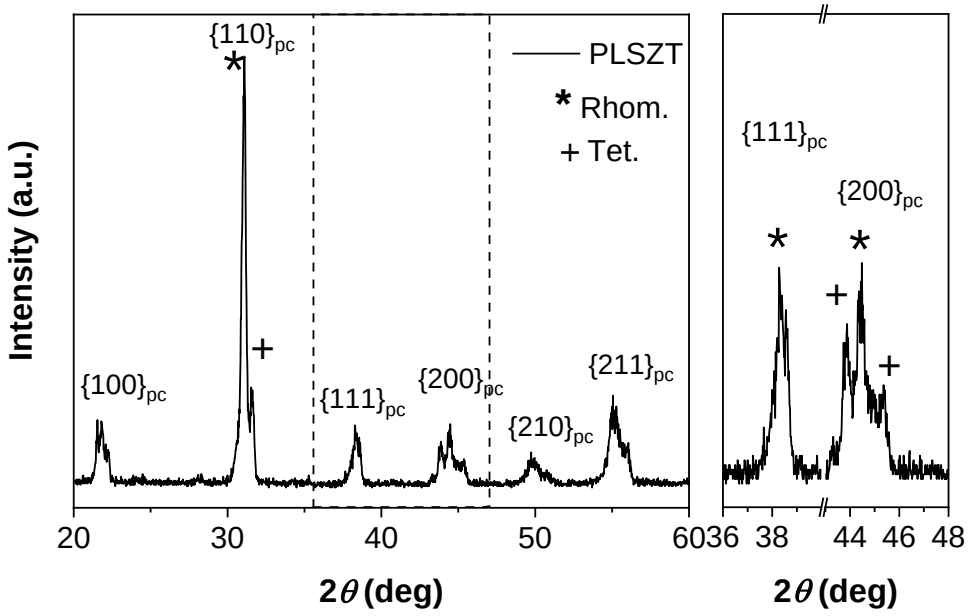

Figure 4-4 XRD patterns for the PLSZT ceramics sintered at 1250 ºC for 2 h.

4.1.2 Density and microstructure

The selected compositions of undoped and doped PZT ceramics with their formula are illustrated in Table 4-1. In addition, a summary of their densities and mean grain sizes are listed.

In general, the hard ceramic (PSZT) only exhibits low density around ~ 7.2 g cm^{-3}. Other ceramics possess high values of density after sintering, greater than 95 % of the theoretical densities (assuming that the theoretical density is equal to ~ 8.07 g cm^{-3})

After doping with 2 mol% of La^{3+}, it can be observed that the densities are slightly decreased after doping as shown in Figure 4-5 This observation is consistent with the finding of L.Pdungsap et.al, who reported that the density of PZT (52/48) decreases slightly with increasing lanthanum content [59]

Table 4-1. Compositional formulas and physical properties of the PZT ceramics.

Composition	Abbreviated	Apparent Density (g cm^{-3})	Mean Grain size (µm)
$Pb_{1.03}(Zr_{0.56}Ti_{0.44})O_3$	PZT	7.74	7.72
$Pb_{1.01}La_{0.02}$ $(Zr_{0.56}Ti_{0.44})O_3$	PLZT	7.70	3.2
$Pb_{1.01}(Sc_{0.02}$ $Zr_{0.54}$ $Ti_{0.44})$ O_3	PSZT	7.2	0.5
$(Pb_{1.01}$ $La_{0.02})$ $(Sc_{0.02}$ $Zr_{0.54}$ $Ti_{0.44})$ O_3	PLSZT	7.6	3.85

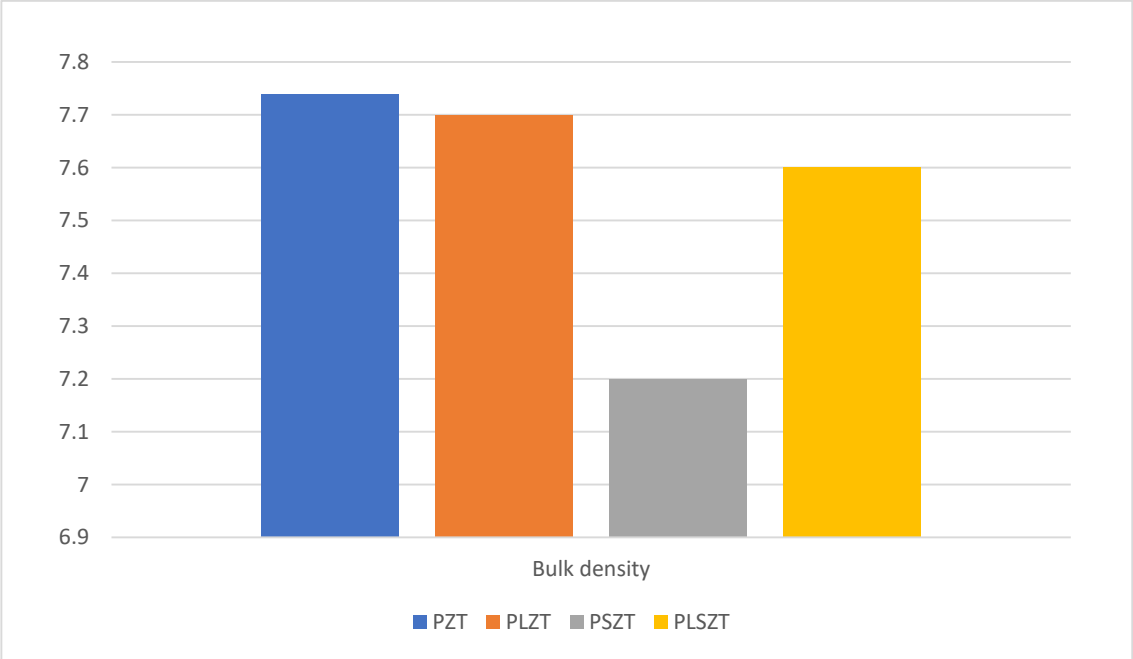

Figure 4-5. Bulk density of undoped and doped ceramics, sintered at 1250 ºC for 2 h

Figure 4-6 shows SEM micrographs of surface morphology of polished and chemically etched surfaces of undoped and doped PZT ceramics. The samples were over etched chemically. Therefore, it can be seen distorted surfaces that exhibited lots of pits. Generally, they revealed dense and homogeneous microstructures exempt the PSZT that exhibited small grain size and higher porosity, relatively. The mean grain sizes values of the ceramics listed in Table 4-1. It measured from the SEM images with scale of 20 µm using the linear intercept method.

A comparison of the SEM images obtained for PZT and PLZT ceramics displays that the average grain sizes of the PZT ceramics were reduced to less than half after doping with La. This observation supports the results of the earlier studies in which the grain size decreased sharply from ~7 μm to even lower ~3 μm when PZT ceramics were doped with 2% La [60]. Langman et al. [61] assigned this grain size reduction to the solid solution impurity drag mechanism, which considers that the presence of the La^{3+} ion concentration gradient at grain boundaries causes blocking of grain boundary mobility and subsequently leads to slower grain growth.

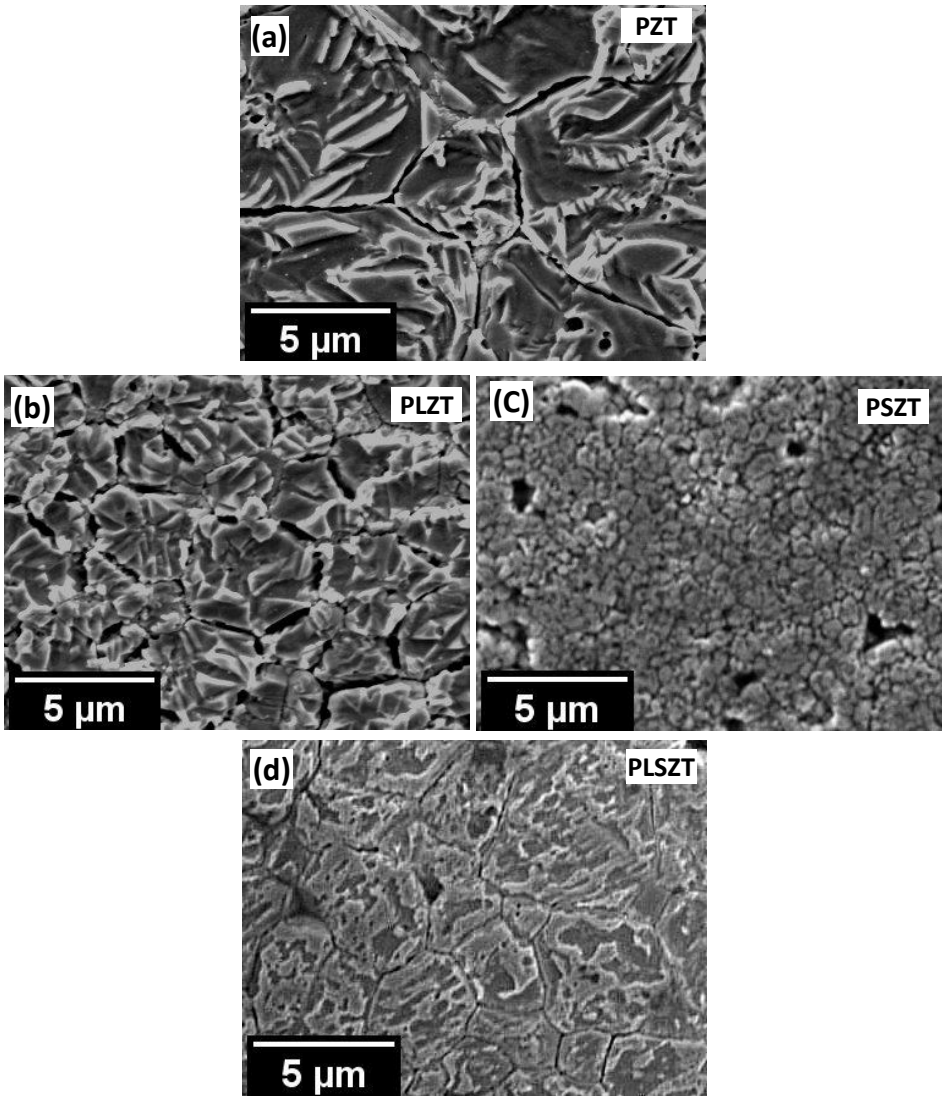

Figure 4-6. SEM micrographs of surface morphology of polished and chemically etched surfaces of undoped and doped PZT ceramics: (a) Undoped PZT, (b) La- doped PZT, (c) Sc- doped PZT, and (d) La-Sc doped PZT

4.2 Electrical properties

4.2.1 Relative permittivity (or dielectric constant) and dielectric loss

Figure 4-7 shows frequency-dependence of dielectric loss and relative permittivity (ε_r) of hard and complex ceramics in range between 100 and 1000 kHz, at room temperature. Overall, both ceramics demonstrated dielectric constant value stability with frequency. However, the hard ceramic has higher values in comparison with those of ceramics with complex doping. Furthermore, both display decreasing in these values with increasing frequency. From 100 kHz to 1000 kHz, ε_r values of PSZT and PLSZT ceramics decreasing from 3450 to 3300 and from 525 to 430, respectively. This is owing to the effects of interfacial, orientation, and ionic polarization, which appear completely where these dielectric constant values at low frequencies are particularly high. On the other hand dielectric loss increase as frequency increase.

The reduction of ε_r values with increasing frequency can be explained as follow; The orient polar group is relatively slow, This is because these consecutive polarizations cannot 'keep up' with the alternating field. The polarization direction cannot remain aligned with the field, and this polarization process no longer contributes to dielectric polarization. As a result, the values of the dielectric constant fall with increasing frequency, as is common in other insulators.

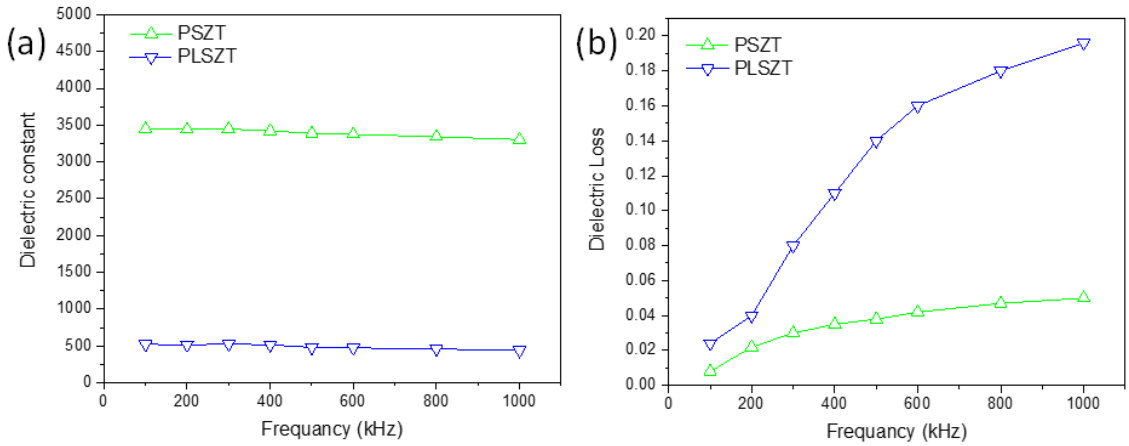

Figure 4-7. Frequency-dependence of dielectric constant for soft and hard ceramics.

On the other hand, Figure 4-8 (a) illustrates the effect of composition on dielectric constant at 100 kHz and at room temperature. It is evident that the highest ε_r value obtained in hard ceramic (PSZT) around 3450. This can be ascribed to the high porosity of the sample relatively as can be seen from SEM images, where it causes increasing in polarization which results from interstitial shipments at low frequencies.

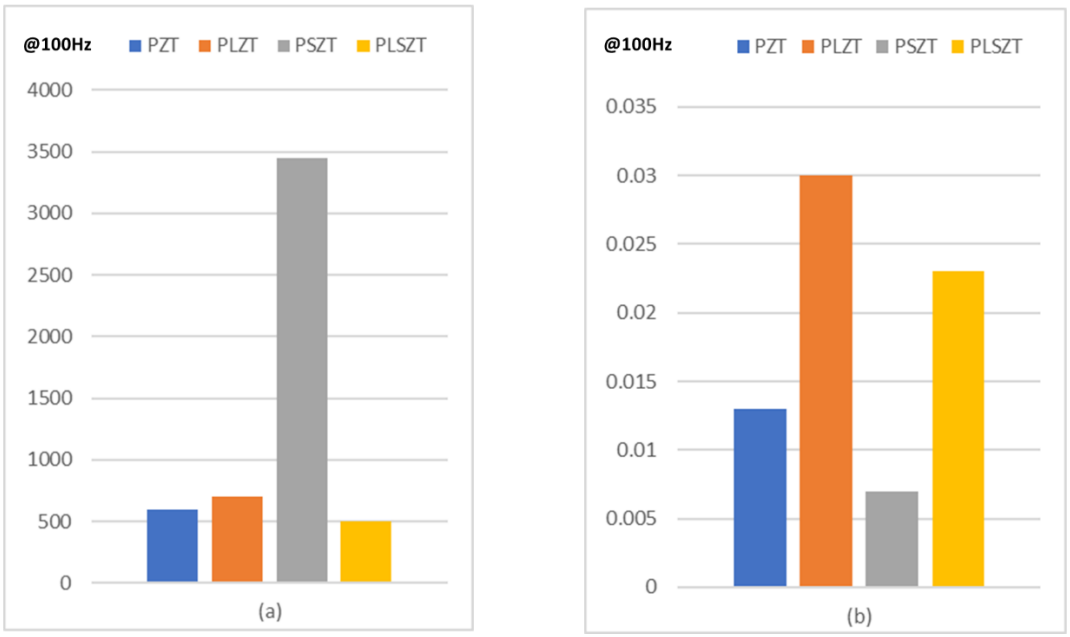

Figure 4-8. Inflenence of donar, acceptor and complex doping on (a)dielectric constant (b) Dielectric loss of PZT ceramic.

the effect of composition on dielectric loss at 100 kHz and at room temperature illustrates in Figure 4-8 (b). It is evident that the lowest tanδ value obtained in hard ceramic (PSZT) around 0.007

4.2.2 Dielectric breakdown

The effect of voltage elevating average on dielectric strength of hard and complex doped ceramics is presented in Figure 4-9. With increasing voltage, both ceramics show a progressive increase in dielectric strength values. Lower dielectric strength values with slow voltage elevating average about 0.5 kV/sec (i.e., long time) can be attributed to heat generation from leakage currents. It is well known that applying a voltage over an extended period of time increases the likelihood of an electrothermal breakdown, since the increasing of local temperature decreases the insulating properties of materials. Furthermore, when materials are exposed to high voltage for an extended period of time, the cumulative effects of collision (chemical and electrochemical) and corrosion occur, destroying the materials and speeding up the breakdown by heating.

On the other hand, higher values of dielectric strength were obtained at high voltage elevating average, where an increase in the voltage elevating average reduces the time required for two consecutive collisions of the same electron due to the acquisition of electrons to sufficient energy, speeding the process of ionization and thus speeding the breakdown, resulting in an increase in dielectric strength values.

We see irregularities in some areas of the overall behavior, and the cause is linked to faults in the bulk materials or homogenous weaknesses of each testing site in the sample. [22, 23, 62].

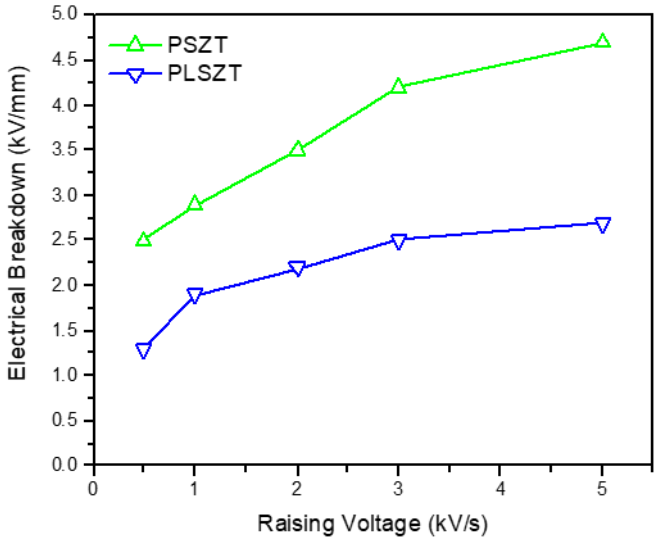

Figure 4-9. Dielectric strength versus voltage elevating average for hard and complex doped ceramics.

4.2.3 Electrical conductivity

The influence of frequency on the electrical conductivity for hard and complex ceramics is illustrated in Figure 4-10 Generally, the electrical conductivity changes linearly with frequency. This is due to a fact at high frequency the capacitive reactance of the sample decreases; hence the impedance is reduced, which causes an increase in the ac conductivity of the sample. $\sigma_{AC}*10^{-7}(S.m)^{-1}$

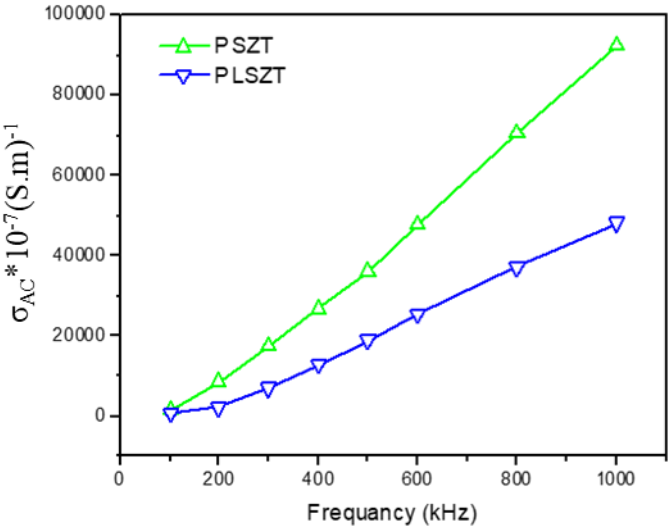

Figure 4-10. Evolution of the electrical conductivity as a function of frequency for soft and hard ceramics.

Chapter Five

Conclusions and Future work

5 Conclusions and Future work

5.1 Conclusions

The ceramics were synthesized by solid state reaction. All samples show dense and homogeneous microstructures uniform ceramics exempt PSZT ceramic displays small grain size, relatively. Previous studies show that decreasing grain size improves dielectric breakdown strength (DBS), which in turn improves energy storage qualities. Therefore, it can be expect increasing in the energy storage values in the sample with complex doping as a result of grain size-reduction.

XRD results show that the addition of Sc^{+3} induce phase transformation and formation coexistence region consist of tetragonal and rhombohedral phases. This region was recognized in both compositions (PSZT) (PLSZT). Hard ceramic (Sc doped PZT) exhibited highest values of relative permittivity and lowest dielectric loss at frequency of 100 kHz.

5.2 Future work

1. Preparation a new composition having different percentages of dopant.
2. Carry out full-pattern refinement using Topas software for all prepared ceramic powders in order to confirm the crystal structure and the phase fraction.
3. Complete electrical characterization including temperature dependence of relative permittivity in order to identify any possible phase transformation in addition to specify the influence of dopants on the Cuire temperature.
4. Furthermore, investigate the influence of dopants on the electrical hysteresis behavior by conducting the P-E hysteresis measurements.

6 Reference

1. Kang, m.-g., et al. Recent progress on pzt based piezoelectric energy harvesting technologies. In actuators. 2016. Mdpi.
2. Izyumskaya, n., et al., processing, structure, properties, and applications of pzt thin films. Critical reviews in solid state and materials sciences, 2007. 32(3-4): p. 111-202.
3. Scott, j.f. And c.a. Paz de araujo, ferroelectric memories. Science, 1989. 246(4936): p. 1400-1405.
4. Tong, s., et al., lead lanthanum zirconate titanate ceramic thin films for energy storage. Acs applied materials & interfaces, 2013. 5(4): p. 1474-1480.
5. Li, q., et al., flexible high-temperature dielectric materials from polymer nanocomposites. Nature, 2015. 523(7562): p. 576-579.
6. Harari, b., development of high capacitance films for electrical energy storage using electrophoretic deposition of batio3 on ultrasonically etched ni. 2012: queen's university (canada).
7. Do, d.-h., investigation of ferroelectricity and piezoelectricity. 2006, university of wisconsin-madison.
8. Frederick, j., strains and polarization developed during electric field-induced antiferroelectric to ferroelectric phase transformations in lead zirconate-based ceramics. 2010: iowa state university.
9. Bharadwaj, s., s. Varma, and b. Wani, electroceramics for fuel cells, batteries and sensors. Functional materials, 2012: p. 639-674.
10. Aggarwal, m., et al., pyroelectric materials for uncooled infrared detectors: processing, properties, and applications. 2010.
11. Moulson, a.j. And j.m. Herbert, electroceramics: materials, properties, applications. 2003: john wiley & sons.
12. Baker, j., m.f. Haider, and r. Raihan, effect of manufacturing on the dielectric properties of composite materials. 2004.
13. Barsoum, m., fundamentals of ceramics, fundamentals of ceramics. New york: mc graw-hill companies. Doi, 2002. 10: p. 0750309024.
14. Amsc, n. And a.a. Cmps, composite materials handbook. Polymer matrix composites materials usage, design, and analysis, 2002.
15. Mitchell, b.s., an introduction to materials engineering and science for chemical and materials engineers. 2004: john wiley & sons.
16. Al-fouadi, a., dielectric properties of local clay-based cordierite ceramics. Al mustansiriyah university, ph. D. Thesis, 2007.
17. Allen, p.b., properties of materials for electrical engineers by kj pascoe. Reviewed by. American journal of physics, 1975. 43(10): p. 929-933.
18. Lawrence, h. And v. Vlack, elements of materials science and engineering. 1989, wesley: addison.
19. Barber, p., et al., polymer composite and nanocomposite dielectric materials for pulse power energy storage. Materials, 2009. 2(4): p. 1697-1733.
20. Song, s. And g. Paulino, internationaljournal of solids and structures. 2006.
21. Staněk, j., electric melting of glass. Vol. 1. 1977: elsevier science & technology.
22. Bunget, i. And m. Popescu, physics of solid dielectrics. Materials science monographs, 1984. 19.

23. Kuffel, j. And p. Kuffel, high voltage engineering fundamentals. 2000: elsevier.
24. Haertling, g.h., ferroelectric ceramics: history and technology. Journal of the american ceramic society, 1999. 82(4): p. 797-818.
25. Zhang, y., et al., energy storage and electrocaloric cooling performance of advanced dielectrics. Molecules, 2021. 26(2): p. 481.
26. Mukherjee, d., growth and characterization of epitaxial thin films and multiferroic heterostructures of ferromagnetic and ferroelectric materials. 2010: university of south florida.
27. Hao, x., et al., a comprehensive review on the progress of lead zirconate-based antiferroelectric materials. Progress in materials science, 2014. 63: p. 1-57.
28. Li, w., et al., high piezoelectric d_{33} coefficient in $(ba_{1-x}ca_x)(ti_{0.98}zr_{0.02})o_3$ lead-free ceramics with relative high curie temperature. Materials letters, 2010. 64(21): p. 2325-2327.
29. Li, j.-f., et al., $(k,na)nbo_3$-based lead-free piezoceramics: fundamental aspects, processing technologies, and remaining challenges. Journal of the american ceramic society, 2013. 96(12): p. 3677-3696.
30. Rödel, j., et al., transferring lead-free piezoelectric ceramics into application. Journal of the european ceramic society, 2015. 35(6): p. 1659-1681.
31. Shrout, t.r. And s.j. Zhang, lead-free piezoelectric ceramics: alternatives for pzt? Journal of electroceramics, 2007. 19(1): p. 113-126.
32. Panda, p.k. And b. Sahoo, pzt to lead free piezo ceramics: a review. Ferroelectrics, 2015. 474(1): p. 128-143.
33. Hong, c.-h., et al., lead-free piezoceramics – where to move on? Journal of materiomics, 2016. 2(1): p. 1-24.
34. Maqbool, a., et al., structural, ferroelectric and field-induced strain response of nb-modified $(bi_{0.5}na_{0.5})tio_3$-$srzro_3$ lead-free ceramics. Ferroelectrics, 2015. 488(1): p. 23-31.
35. Haertling, g.h., ferroelectric ceramics: history and technology. Journal of the american ceramic society, 1999. 82(4): p. 797–818.
36. Panda, p.k., review: environmental friendly lead-free piezoelectric materials. Journal of materials science, 2009. 44(19): p. 5049-5062.
37. Jin, l., broadband dielectric response in hard and soft pzt: understanding softening and hardening mechanisms, in phd thesis, swissfederal institute of technology-epfl. 2011: switzerland.
38. Hu, w., x. Tan, and k. Rajan, combinatorial processing libraries for bulk bifeo3–pbtio3 piezoelectric ceramics. Applied physics a, 2010. 99(2): p. 427-431.
39. Horchidan, n., et al., a comparative study of hard/soft pzt-based ceramic composites. Ceramics international, 2016. 42(7): p. 9125-9132.
40. Caceres, j.a.s., et al., study of structural and electric properties of the pzt 52/48 doped with er+ 3. Materials research, 2019. 22.
41. Pereira, m., a. Peixoto, and m. Gomes, effect of nb doping on the microstructural and electrical properties of the pzt ceramics. Journal of the european ceramic society, 2001. 21(10-11): p. 1353-1356.
42. Sahoo, b. And p.k. Panda, effect of lanthanum, neodymium on piezoelectric, dielectric and ferroelectric properties of pzt. Journal of advanced ceramics, 2013. 2(1): p. 37-41.
43. Al-aaraji, m.n., nanostructured ferroelectric ceramics and coatings. 2018: the university of manchester (united kingdom).

44. Sangawar, s., et al., fe doped hard pzt ceramics for high power sonar transducers. Materials today: proceedings, 2015. 2(4-5): p. 2789-2794.
45. Mahato, d., r. Chaudhary, and s. Srivastava, effect of na on microstructure, dielectric and piezoelectric properties of pzt ceramic. Journal of materials science letters, 2003. 22(22): p. 1613-1615.
46. Sun, h., et al., the effect of mn/nb doping on dielectric and ferroelectric properties of pzt thin films prepared by sol–gel process. Journal of sol-gel science and technology, 2015. 74(2): p. 378-386.
47. Moradi, z., s.z. Jahromi, and m. Ghaedi, design of active photocatalysts and visible light photocatalysis, in interface science and technology. 2021, elsevier. P. 557-623.
48. Bhattarai, m.k., et al., effect of off-center ion substitution in morphotropic lead zirconate titanate composition. Journal of applied physics, 2017. 121(19): p. 194102.
49. Bhattarai, m.k., s.p. Pavunny, and r.s. Katiyar, effect of la and sc co-doping on dielectric and ferroelectric properties of pzt for energy storage capacitors. Journal of applied physics, 2021. 130(3): p. 034103.
50. Zak, a., et al., effect of y 3 and nb 5 co-doping on dielectric and piezoelectric properties of pzt ceramics. Materials science-poland, 2010. 28(3).
51. Waanders, piezoelectric_ceramics__properties_and_applications. 2003.
52. Jackson, t.n., synthesis and processing of ferroelectric pzt powders, ceramics and films. 2006.
53. Greskovich, c., milling, in treatise on materials science & technology. 1976, elsevier. P. 15-33.
54. Matsuo, y., formation of lead zirconate-lead titanate. 1965.
55. Chandratreya, s., r.m. Fulrath, and j.a. Pask, reaction mechanisms in the formation of pzt solid solutions. Journal of the american ceramic society, 1981. 64(7): p. 422-425.
56. Nwaogu, u.c. And n.s. Tiedje, foundry coating technology: a review. Materials sciences and applications, 2011. 2(08): p. 1143.
57. Jin, l., broadband dielectric response in hard and soft pzt. 2011, epfl.
58. Yu, y., field-induced antiferroelectric-ferroelectric phase switching behavior in lead strontium zirconate titanate ceramics. 2000, university of cincinnati.
59. Pdungsap, l., et al., optimized conditions for fabrication of la-dopant in pzt ceramics. Sensors and actuators a: physical, 2005. 122(2): p. 250-256.
60. Hammer, m. And m.j. Hoffmann, detailed x-ray diffraction analyses and correlation of microstructural and electromechanical properties of la-doped pzt ceramics. Journal of electroceramics, 1998. 2(2): p. 75-84.
61. Langman, r.a., r.b. Runk, and s.r. Butler, isothermal grain growth of pressure-sintered plzt ceramics. Journal of the american ceramic society, 1973. 56(9): p. 486-488.
62. Kroschwitz, j.i., electrical and electronic properties of polymers: a state-of-the-art compendium. 1988: wiley-interscience.

الخلاصة:

تم تحضير مواد فيروكهربائية والمكونة بشكل رئيسي من الرصاص Lead zirconate titanate (PZT) باستخدام الطريقة التقليدية (طريقة تفاعل الحالة الصلبة)، بالحالة النقية وبالتشويب بأيونات مختلفة. التركيب الاساسي الي تم اختياره يقع في منطقة ال Rhombohedral في مخطط التوازن PZ-PT وحسب الصيغة الكيميائية $Pb_{1.03}(Zr_{0.56}Ti_{0.44})O_3$ والتي بالقرب من منطقة ال Morphotropic Phase Boundary (MPB) التي تتميز باحتوائها على نوعين من البنية البلورية لمادة ال PZT الفيروكهربائية، هما (Tetragonal) وال (rhombohedral). تم اتباع إستراتيجيات مختلفة في التشويب لمعرفة تأثير الايونات المشوبة على الخصائص البنيوية والتركيبية والكهربائية على مادة ال PZT الفيروكهربائية. الطريقة الاولى تضمنت التشويب بأيون ال La^{3+} في الموقع A من المادة الأم حسب الصيغة ABO_3 المميزة لبنية البيروفسكايت، أي التشويب يكون باستبدال جزئي لأيون ال Pb^{+2} .بهذا يكون التشويب مانح والمادة المنتجة تُوصف بانها Soft. اما الطريقة الثانية، تضمنت التشويب بأيون ال Sc^{3+} في الموقع B من المادة الأم أي التشويب يكون باستبدال جزئي لأيون ال Zr^{+4} .بهذا يكون التشويب كاسب والمادة المنتجة تُوصف بانها Hard. تم اختيار ال Zr^{+4} وليس ال Ti^{+4} كموقع للتشويب كون ال Zr^{+4} يعمل على تثبيت البنية البلوية rhombohedral وهذا غير مطلوب، كون الهدف المطلوب هو احداث تحول طوري في المادة. . اما الطريقة الثالثة، تضمنت التشويب بأيون ال La^{3+} وال Sc^{3+} في الموقعA و B في نفس الوقت في المادة الأم أي التشويب يكون باستبدال جزئي لأيونات ال Pb^{+2} وال Zr^{+4} ، على التوالي. بهذا يكون التشويب مانح وكاسب في نفس الوقت والمادة المنتجة تُوصف بانها Complex doped materials.

العينات بمختلف التراكيب أظهرت بنية مجهرية كثيفة ومتجانسة باستثناء PSZT حيث تميزت الاخيرة بحجم حبيبي صغير نسبياً. فيما بينت تحاليل حيود الاشعة السينية ان اضافة ال Sc^{3+} أو ال $Sc^{3+} + La^{3+}$ تساعد على احداث تحول طوري، حيث كشفت التحاليل ظهور طور ال(Tetragonal) الى جانب طور ال (rhombohedral). فيما يخص الفحوصات الكهربائية، أظهرت النتائج ان السيراميك الصلب المشوب بال Sc^{+3} يمتلك أعلى قيم للسماحية النسبية وأدنى خسارة عازلة عند تردد 100 كيلو هرتز.

جمهورية العراق
وزارة التعليم العالي والبحث العلمي
جامعة بابل
كلية هندسة المواد
قسم هندسة السيراميك ومواد البناء

دراسة خصائص البنيوية والكهربائية للسيراميك المُشوب بأيونات مانحة وكاسبة

رسالة مقدمة إلى

قسم هندسة السيراميك ومواد البناء في كلية هندسة المواد/ جامعة بابل

كجزء من متطلبات نيل درجة الدبلوم العالي في هندسة السيراميك

أعدت من قبل

عبد المجيد حميد عكلة

بكالوريوس هندسة سيراميك ومواد بناء - 2019

بإشراف

د. محمد ناجي حسن الأعرجي

2022